University **POLITEHNICA** of Bucharest

Doctoral School of **Applied Science**

PhD Thesis Summary

Electrodeposition of nickel and tin based alloys from deep eutectic solvents for electronic applications

PhD candidate: Rosoiu Sabrina Patricia

Supervisors

Prof. dr. rer.nat. Marian Enachescu

and

Emeritus Prof.dr.ing. Teodor Visan

Bucharest, September 2021

Table of contents

Keywords: *electrodeposition, direct current, pulse current, Deep Eutectic Solvents, Ionic Liquids, nickel-tin alloy, nickel-tin reduced graphene composite, tin-copper-nickel alloy, corrosion, salt spray test, scanning vibrating electrode technique*

The present abstract briefly presents the content of chapters 4-9, related to the original contributions and the conclusions of the entire work. The numbering of the figures, tables, equations and references corresponds to that of the thesis.

Introduction

The electrochemical co-deposition of metals is of great interest since the resulted alloys exhibit superior properties compared to their corresponding individual components in terms of corrosion resistance, mechanical properties, and thermal stability [1]. Usually, the alloys are synthesized involving water-based electrolytes.

The electrodeposition of tin and some of its alloys has attracted a great interest due to their large range of industrial applications including light engineering and electronics. Alloying tin with other elements may improve its corrosion resistance and limits the formation of tin whiskers and tin pest which represent the major limitation of using bare Sn metal in electronic industry. Tin pest is the allotropic phase transformation of white β-tin to structurally weak gray powdery α-tin at relatively low temperatures (below 13.2 ºC). The α-tin structure is not acceptable in electronic systems [2]. On the other side, tin whiskers are filaments that emerge from tin coatings after deposition. They can grow several mm and cause the failure of electronic systems due to short circuits formed as unwanted electrical connections [3].

Nickel has been widely applied as protective coatings due to its corrosion performance. It is also used as undercoat for noble metal finishes, especially in electronic industry during the manufacturing of printed circuit boards (PCB). The main disadvantage of Ni is that is allergenic and cause dermatitis [4-5] . Because of that it should not be used in jewelries and as decorative coatings in other objects that are in contact with human skin. However, alloying nickel with other elements can prevent nickel allergy [5].

Ni-Sn and Sn-Cu-Ni alloys found applications in electronic industry. In general, tin and nickel-based alloys are synthetized by electrodeposition from aqueous based electrolyte. However, the electrodeposition from water solution is challenging. Tin is not stable in aqueous solution since it is easily oxidized from Sn^{2+} to Sn^{4+} that leads to the formation of sludge, destabilizing the plating bath. To avoid the oxidation of divalent tin to tetravalent tin, additives must be added to the electrolyte to minimize the oxidation process [8]. Furthermore, special attention should be given to stirring, air flow and anode material since the stability of stannous is relying on these factors too. In addition, electrodeposition of nickel and tin alloys is difficult in water-based solution due to the large difference between the standard reduction potential of Sn (-0.14 V vs. SHE), Cu (+0.34 V vs SHE) and Ni (-0.25 V vs SHE). For alloy electrodeposition, the deposition potential of the nobler component must be shifted to a more negative value, which is in general achieved by the addition of a suitable complex agent to the plating bath that brings the potential closer [9].

A green alternative to the traditional complex water-based plating baths is represented by the so-called “deep eutectic solvents”. They are a class of ionic liquids that are non-sensitive to water, biodegradable, exhibit wide potential window, conductivity, and high viscosity [10]. Adequate deposits can be obtained without the use of supplementary additives, leading to very simple plating baths containing just the metallic ions that need to be deposited. The use of these ionic media allows the electrochemical deposition of alloys that are not possible to be obtained from aqueous solution without the use of additives, since the potential of the metallic species are more negative than the potential for discharge of H^+ and therefore hydrogen evolution or the difference between them is very high.

Furthermore, the incorporation of carbon-based materials into the matrix of metal and alloy coatings has showed an improvement of their properties such as: hardness, conductivity, and corrosion resistance [11]. According to recent investigations, the dispersion stability of multi-walled carbon nanotubes (MWCNTs) or GO is significantly improved in the deep eutectic solvents.

The aim of the thesis is to study the electrodeposition of Ni-Sn and Sn-Cu-Ni alloys from air and water stable deep eutectic solvents. The electrodeposition baths are very simple, they just contain the metallic salts without surfactants, antioxidants, brighteners, grain refiners and other additives that are usually added in the water-based plating solutions. In addition, the influence of the incorporation of carbon-based nanomaterials (reduced graphene oxide) on the properties of the Ni-Sn alloys is studied.
A comprehensive investigation of the electrodeposition of these alloys and composites is performed. The nucleation mechanisms and the influence of the plating parameters on the morphology and characteristics of the materials are studied. Special attention is given to the anti-corrosive properties of the films which are investigated at macro-and micro-scale.
Furthermore, this thesis aims to explore the scale-up electrodeposition of the ternary Sn-Cu-Ni alloy from deep eutectic solvents on printed circuit boards (PCB). Since the Sn-Cu-Ni alloy has found applications as solder in electronic industry the behavior of the film under industrial reflowing conditions is also studied.

Chapter IV: Ni-Sn alloys electrodeposition from choline chloride-based ionic liquids in direct and pulsed current

This chapter presents the electrodeposition of Ni-Sn alloys using direct current (DC) and for the first time, pulse current (PC), from deep eutectic solvents (denoted DES), respectively from choline chloride: ethylene glycol eutectic mixtures.

Different amounts of nickel and tin salts have been added to a DES of choline chloride: ethylene glycol (1:2 molar ratio, denoted ILEG), corresponding to three different types of electrolytes: ILEG-$NiSn_1$, ILEG-$NiSn_2$ and ILEG-$NiSn_3$ as shown in Table 4.1.

Table 4.1. Concentration of metal salts dissolved in ILEG.

System Type	Metal Salt, mol/L
ILEG-$NiSn_1$	0.33 M $NiCl_2 \cdot 6H_2O$ + 0.67 M $SnCl_2 \cdot 2H_2O$
ILEG-$NiSn_2$	0.5 M $NiCl_2 \cdot 6H_2O$ + 0.5 M $SnCl_2 \cdot 2H_2O$
ILEG-$NiSn_3$	0.67 M $NiCl_2 \cdot 6H_2O$ + 0.33 M $SnCl_2 \cdot 2H_2O$

All the mixtures were in a liquid state at room temperature, with a green colour, and electrical conductivities in the range of 2–12 mS/cm for temperatures between 25–80 °C. Nickel-tin (Ni-Sn) alloys have been electrodeposited under DC conditions on Cu substrates in a galvanostatic mode, at different current densities. The obtained deposits were bright, grey, and adherent to the copper substrates.
The coatings exhibited different calculated thicknesses (using Faraday's law) in the range of 4 to 10 µm, depending on the applied current density.

Figure 4.6 shows examples of SEM micrographs of Ni-Sn deposits obtained from the different ILEG-NiSn systems. As shown in Figure 4.6, no dendritic growth was observed. Different surface morphologies defined by acicular (ILEG-$NiSn_2$), circular (ILEG-$NiSn_3$), and quasi-circular (ILEG-$NiSn_1$) features have been identified, as a result of the variation of current density and the electrolyte nature.

The elemental composition of the films, evaluated from EDX, remains almost constant independently on the electrodeposition parameters. The weight percentages determined by EDX are around 32 wt.% Ni and 68 wt.% Sn (approximately 1:1 atomic Ni:Sn).

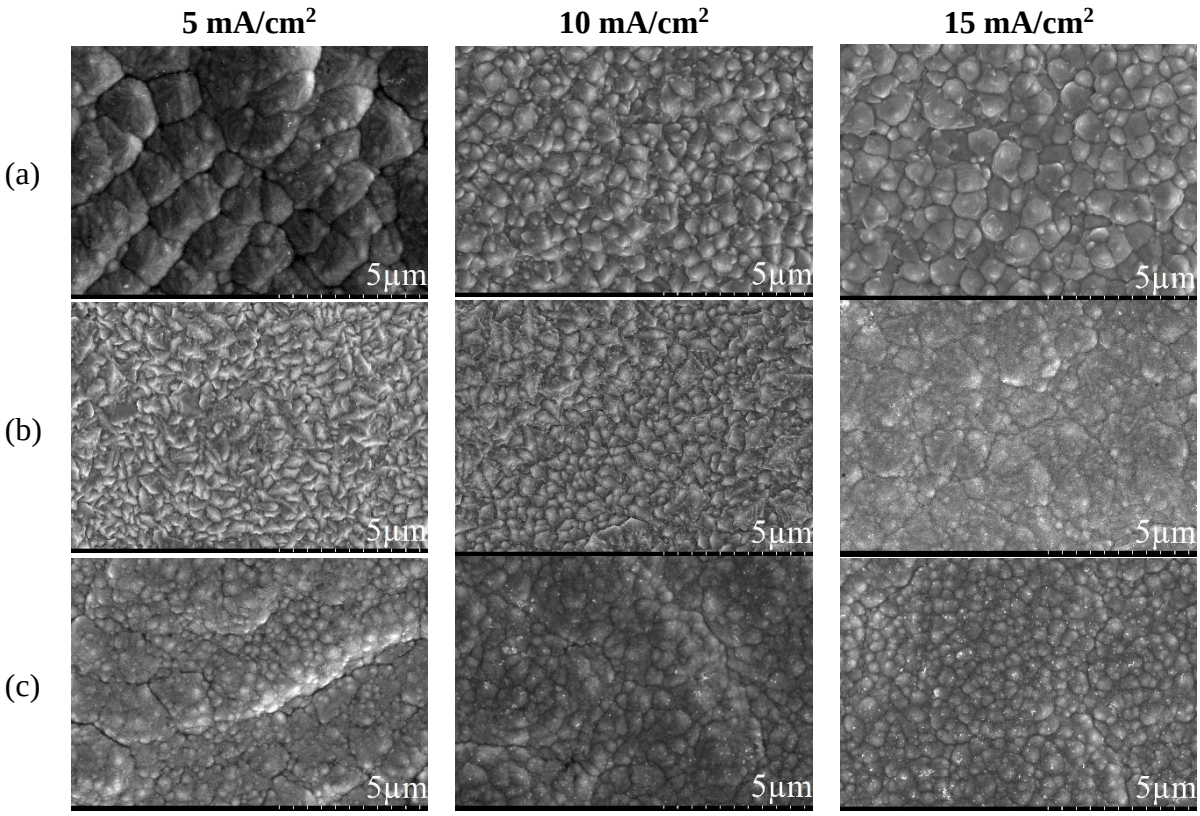

Figure 4.6. SEM micrographs of Ni-Sn alloys electrodeposited in the DC regime at different current densities from different types of electrolytes: (a) ILEG-NiSn1, (b) ILEG-NiSn2, and (c) ILEG-NiSn3.

The XRD patterns obtained for the samples prepared under DC electrodeposition from different types of electrolytes, see Figure 4.9. For the Ni-Sn alloy prepared from ILEG-NiSn1 electrolyte, the XRD pattern was plotted using a logarithmic scale in order to show the low intensity peaks. The diffraction peaks at 2θ = 30.50°, 43.77°, 54.61°, 60.15°, 63.61°, 72.66°, 80.69°, and 89.92° were assigned to NiSn metastable phase and the peaks at 2θ = 44.32°, 50.48°, and 74.10° were attributed to the copper substrate (card No.: 00-004-0836) [31].

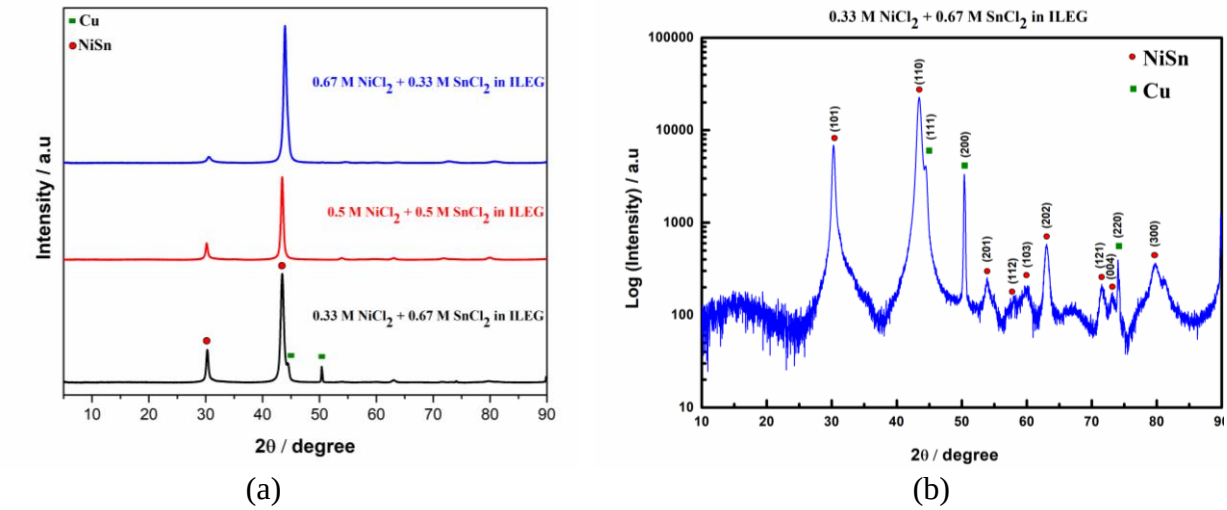

Figure 4.9. X-ray diffraction patterns of electrodeposited NiSn alloys on copper substrate: (a) linear scale and (b) logarithmic scale.

The formation of the metastable phase NiSn is independent on the concentration ratio of metal salts in the electrolyte, and it was confirmed by heat treatment studies using differential scanning calorimetry. As it can be seen in Figure 4.12, one exothermic peak is observed at 292 °C. This peak is associated with the transformation of NiSn in both Ni_3Sn_2 and Ni_3Sn_4 phases, which confirms that the metastable phase was obtained by electrodeposition, as described by Dutta and Clarke [35]. This metastable phase is not presented in the phase diagram. After completing the phase transformation, the sample was subjected to a second thermal cycle (2nd DSC measurement), where no peak was observed, which indicates the irreversibility of the process.

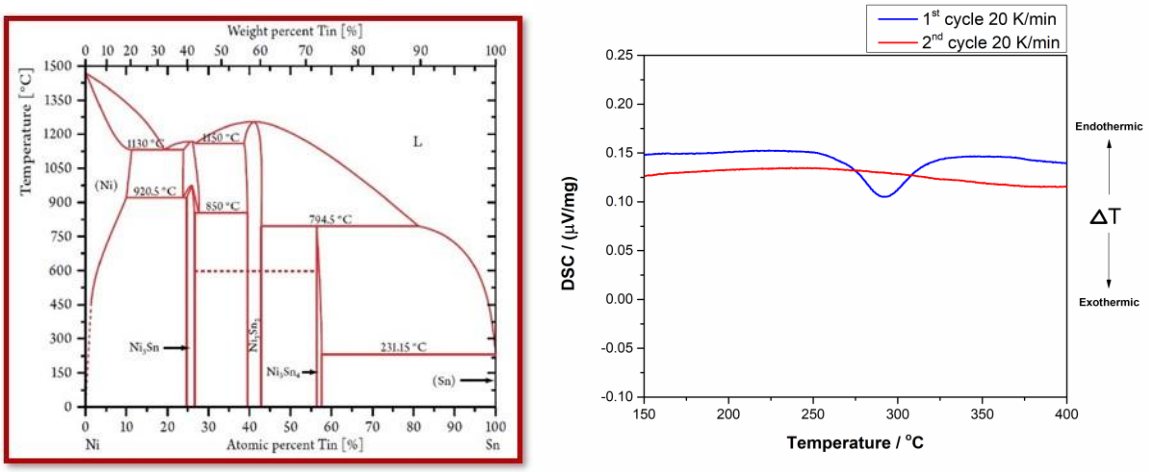

Figure 4.12. Phase diagram of Ni and Sn (left)[44] and differential scanning calorimetry (DSC) curves (right) for the Ni-Sn sample prepared in DC from the ILEG-$NiSn_2$ system.

The second part of the study was focused on the electrodeposition of Ni-Sn coatings in pulse current plating. To the best of our knowledge, this is the first time when nickel tin alloys were electrodeposited from deep eutectic solvents in pulse current.

The surface morphology and the composition of the obtained Ni-Sn deposits were characterized by SEM-EDX. As shown in Figure 4.14, there are no noticeable differences in the surface morphology between the coating prepared in direct current and the ones obtained in pulse current electrodeposition conditions.

The detailed applied operating parameters are presented in Table 4.3

Table 4.3. Operating parameters for the electrodeposition of Ni-Sn alloys from ILEG-$NiSn_2$ system under direct current (sample DC) and pulse current (samples P1, P2, and P3).

Electrolysis Parameter	**NiSn-DC**	**NiSn-P1**	**NiSn-P2**	**NiSn-P3**
On- and off-time durations of the pulse (ms)	-	T_{ON} = 5000 T_{OFF} =10,000	T_{ON} = 500 T_{OFF} = 1000	T_{ON} = 50 T_{OFF} = 100
Frequency (Hz)	-	*f = 0.067*	*f = 0.67*	*f = 6.7*
Duty cycle	-	θ = 0.33	θ = 0.33	θ = 0.33
Current density (average density) (mA/cm^2)	*I* = 6.67	i_{av} = 6.67	i_{av} = 6.67	i_{av} = 6.67

[1]T_{ON} and T_{OFF} are the on and off time duration of the pulse.

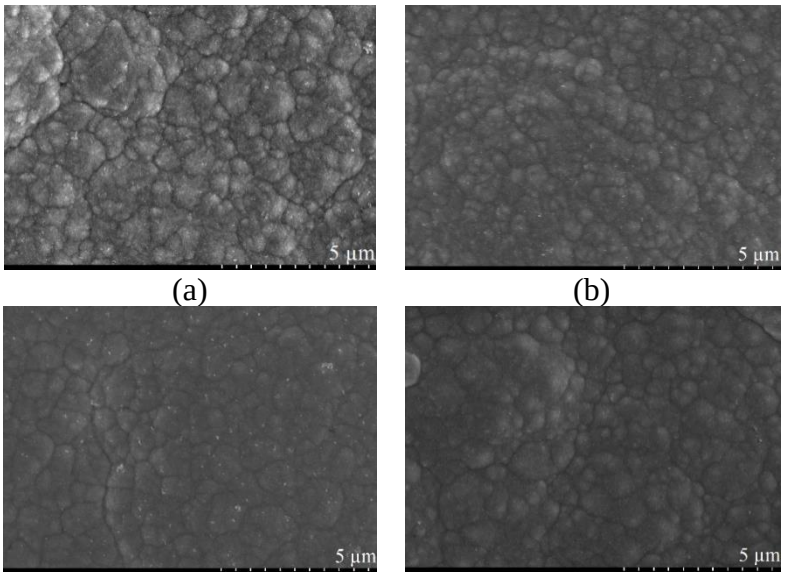

Figure 4.14. SEM micrographs of samples: (a) NiSn-DC, (b) NiSn-P1, (c) NiSn-P2, and (d) NiSn-P3.

All the deposits showed circular grains distributed over the entire surface. The XRD pattern showed the formation of the same NiSn metastable phase.

The micro-mechanical properties of NiSn-DC, NiSn-P1, NiSn-P2, and NiSn-P3 samples were investigated in the cross-section. Table 4.4 shows the Ni-Sn films properties for samples obtained in both DC and PC conditions.

Table 4.4. Effect of direct current and pulse current conditions on the hardness of nickel-tin alloys coatings, electrodeposited from a bath containing 0.5 M $NiCl_2$ + 0.5 M $SnCl_2$ in ILEG.

Film Properties	NiSn-DC	NiSn-P1	NiSn-P2	NiSn-P3
Hardness at 20 mN load (GPa)	8.18 ± 0.42	9.92 ± 0.46	10.24 ± 0.67	12.73 ± 0.75
Reduced Modulus (GPa)	156.60 ± 3.05	154.20 ± 12.07	141.40 ± 17.72	149.71 ± 8.04
Alloy composition (wt. %)	33.54% Ni +66.46% Sn	32.81% Ni +67.19% Sn	30.44% Ni +69.56% Sn	35.09% Ni + 64.91% Sn

[1] The alloy composition was determined by EDX.

As shown in this table, the use of pulse current improves the mechanical properties of the coatings as compared to DC. By increasing the frequency, a gradual increase in the hardness was observed from 9.92 GPa at 0.067 Hz, up to 12.73 GPa at 6.7 Hz. At short on-time, the diffusion layer is not extended completely on the solution, which leads to fine grain deposits that decrease the porosity of the coatings and improve their mechanical properties [42,43].

Chapter V: NiSn-rGO composite electrodeposition from choline chloride-based ionic liquids

This chapter describes the electrodeposition of Ni-Sn alloy/reduced graphene oxide composite coatings (NiSn-rGO) obtained under pulse current electrodeposition conditions from deep eutectic solvents (choline chloride: ethylene glycol eutectic mixtures) containing well-dispersed GO nanosheets.

In order to investigate the composite electrodeposition process, 0.5 M $SnCl_2$ $2H_2O$ and 0.5 M $NiCl_2 \cdot 6H_2O$ as metal precursors and 0.1 g/L GO were added to the ILEG eutectic mixture. For the electrodeposition of NiSn-alloys, the electrolyte contained the same amount of the metallic salts as in the case of the composite material. All prepared media were in liquid state at room temperature.

The influence of the pulse current parameters on the incorporation of the carbonic material into the metallic matrix was investigated. In order to keep the graphene oxide content in the electrolyte constant, ultrasound stirring was used during the pulse electrodeposition process. The T_{ON} time was kept constant, while the T_{OFF} time varied.

The operating parameters set during the electrodeposition of the composite material are presented in Table 5.2.

Table 5.2. Operating parameters for the electrodeposition of NiSn-rGO from ILEG, t = 30 min and a constant peak current density.

Electrolysis Parameter	NiSn-rGO-P1	NiSn-rGO-P2	NiSn-rGO-P3
On- and off-time duration of the pulse	T_{ON} = 500 ms T_{OFF} = 250 ms	T_{ON} = 500 ms T_{OFF} = 500 ms	T_{ON} = 500 ms T_{OFF} = 1000 ms
Frequency (f)	f = 1.33 Hz	f = 1 Hz	f = 0.67 Hz
Duty cycle (θ)	θ = 0.67	θ = 0.5	θ = 0.33
Peak current density (i_p)	i_p = 20 mA/cm^2	i_p = 20 mA/cm^2	i_p = 20 mA/cm^2

T_{ON} and T_{OFF} are the on and off time durations of the pulse.

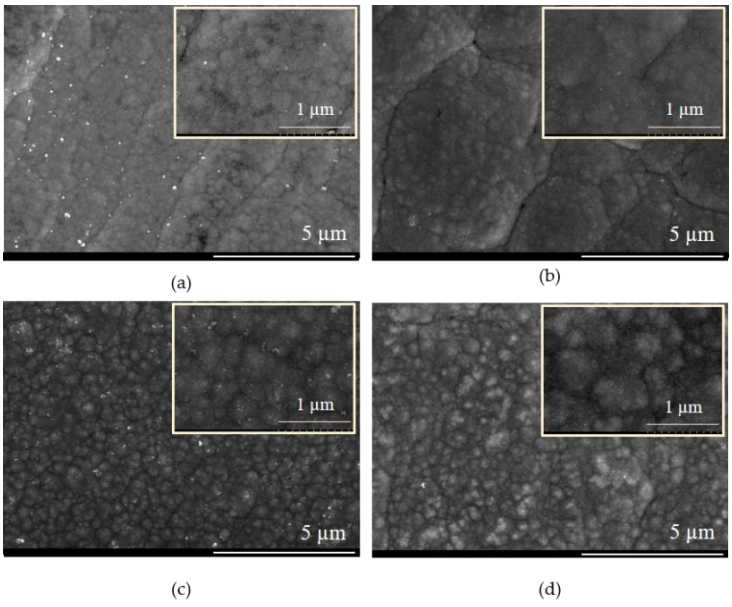

Figure 5.7. SEM micrographs of NiSn alloys obtained at different peak current densities: (a) NiSn-P3.1, (b) NiSn-P3.2, (c) NiSn-P3.3 and (d) NiSn-P3.4.

Considering the optimal pulse plating conditions, T_{ON} = 500 ms and T_{OFF} = 1000 ms, NiSn alloys and NiSn-rGO composite coatings were prepared at several values of the peak current density, set as 10, 15, 20 and 25 mA/cm^2 as it can be seen in the SEM micrographs from Figure 5.7 and 5.8 corresponding to NiSn alloys and NiSn-rGO composite coatings, respectively.

The elemental composition of the coatings was determined using the EDX technique. Values of 65.83 ± 2.11 Sn/31.34 ± 2.13 Ni and 65.65 ± 1.34 Sn/30.51 ± 1.42 Ni ratios of weight percentage were determined for the NiSn alloys and for the composites, respectively.

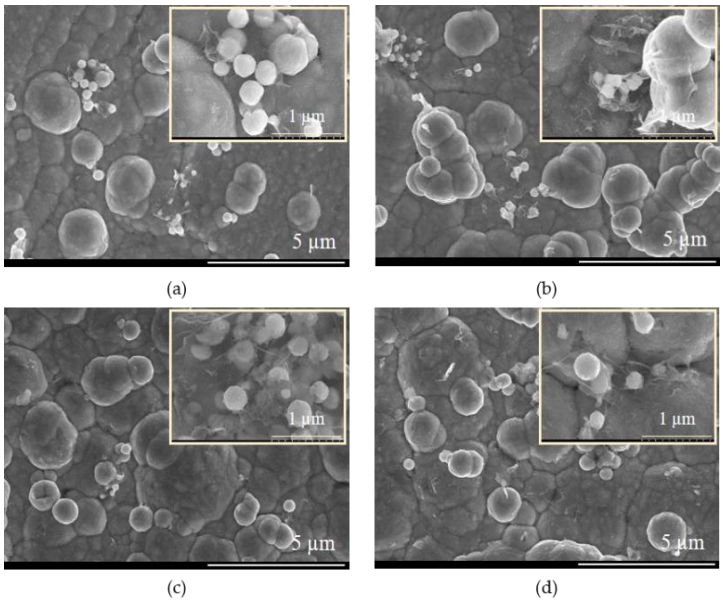

Figure 5.8. SEM micrographs of NiSn-rGO obtained at different peak current densities: (a) NiSn-rGO-P3.1, (b) NiSn-rGO-P3.2, (c) NiSn-rGO-P3.3 and (d) NiSn-rGO-P3.4.

The successful incorporation of the carbon-based material into the metallic matrix has been confirmed by SEM-cross section analysis, as it can be seen in Figure 5.12 and by Raman spectroscopy, as shown in Figure 5.13 illustrating the recorded spectra of the commercial graphene oxide and of the NiSn-rGO-P3.3 composite coating.

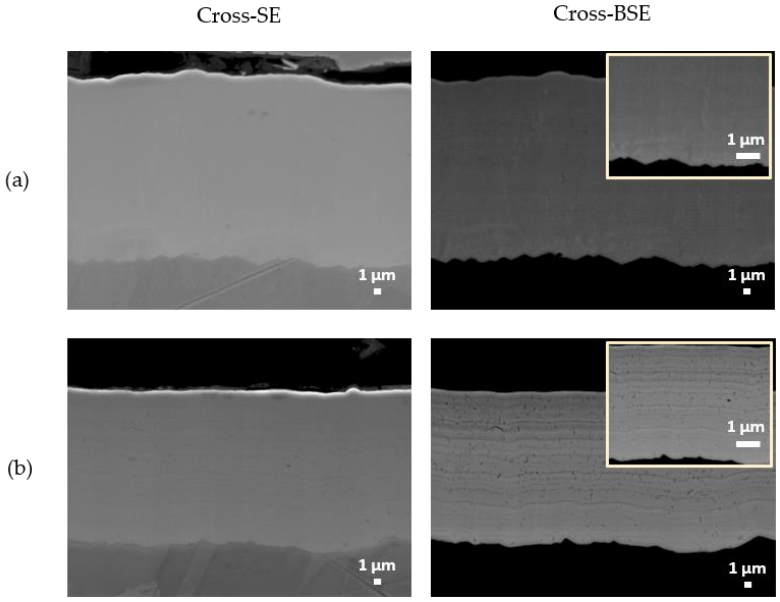

Figure 5.12. SEM micrographs collected with different detectors, secondary electrons (SE) and backscattered electrons (BSE) in the cross-section of: (a) NiSn-P3.3 and (b) NiSn-rGO-P3.3.

From the spectra presented in Figure 5.13, the I_D/I_G ratio of NiSn-rGO was estimated as 1.34, which is higher than that of GO (1.01). The increase in the I_D/I_G ratio suggests the formation of new domains of conjugated carbon atoms as a result of the removal of the oxygen-containing groups, indicating that more defects could have been introduced during the electrochemical reduction process. Moreover, a red shift of the G band is observed in the composite material (1594 cm^{-1}) as compared to GO (1601 cm^{-1}), attributed to the partial recovery of the hexagonal sp^2 carbon network, evidencing the partial electrochemical reduction of GO [31, 47,48].

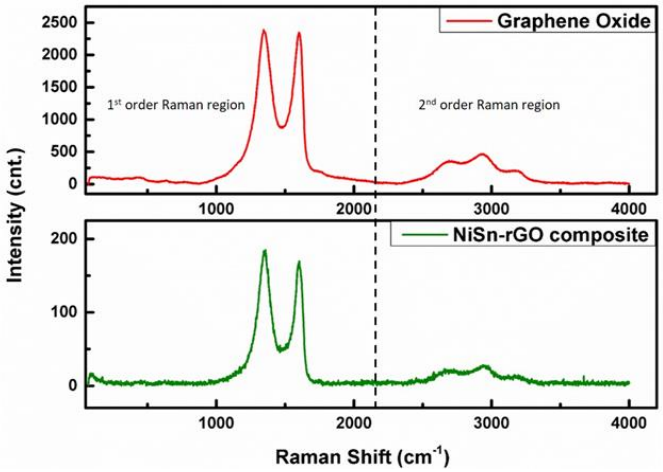

Figure 5.13. Raman spectra of: (top) graphene oxide and (bottom) the composite NiSn-rGO-P3.3.

The XRD patterns of NiSn-P3.3 alloy and NiSn-rGO-P3.3 composite coating are presented in Figure 5.16.

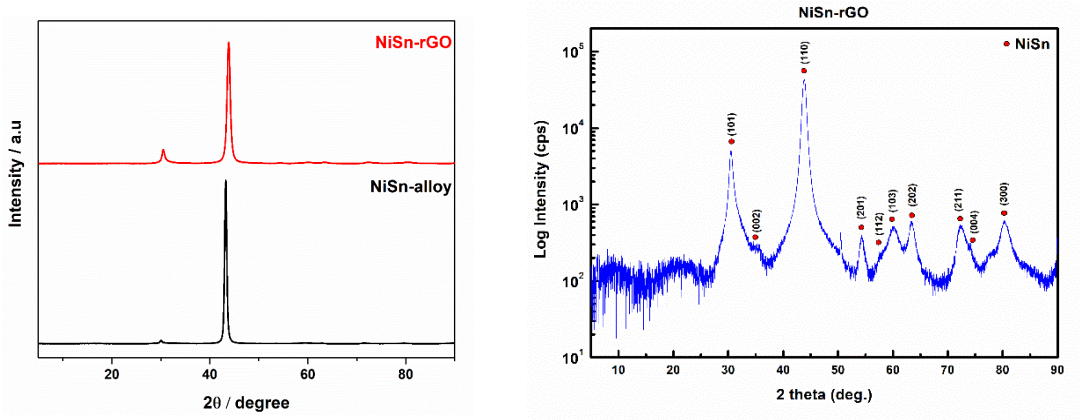

(a) (b)

Figure 5.16. X-ray diffraction patterns of electrodeposited NiSn-P3.3 alloy and NiSn-rGO-P3.3 composite on copper substrate: (a) linear scale and (b) logarithmic scale.

They suggest the formation of the NiSn metastable phase by electrodeposition in both cases [50]. Scherrer's equation was used to determine the crystallite size. A decrease in the crystallite size was observed when graphene was added to the electrolyte from 18.6 nm in the NiSn alloy to 12.1 nm in the composite. This behaviour is consistent with the Raman results. The presence of graphene may increase the nucleation sites and retard the growth of the crystals by affecting the diffusion of the ions to the existing nucleation sites [51].

The nickel-tin alloy (NiSn-P3.3) and the composite coating (NiSn-rGO-P3.3) were examined by atomic force microscopy (AFM) in contact mode. Figures 5.18 shows the topography signal acquired in contact mode on an area of 3 × 3 μm^2 for NiSn alloy and NiSn-rGO composite. The surface roughness increases with the addition of graphene oxide, also in agreement with the findings reported in [31]. Additionally, the topography, lateral force and current signals were acquired simultaneously in contact mode on an area of 3 × 3 μm^2, as illustrated in Figure 5.18. With the conducting atomic force microscopy (C-AFM), using an electrically conductive probe tip in contact mode, it was possible to map the changes in the surface conductivity. The decrease in the electrical conductivity of the composite could be attributed to an imperfect removal of the oxygen groups from the GO sheets.

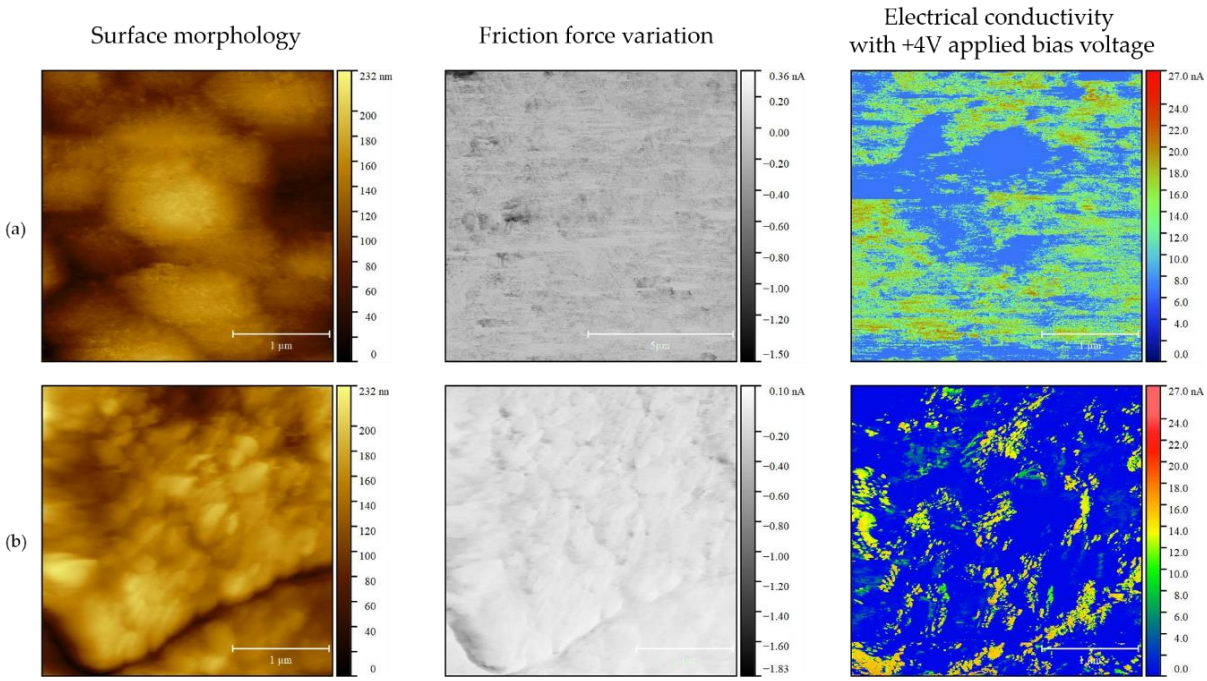

Figure 5.18. The 3 × 3 µm² 2D AFM images of: (a) NiSn-P3.3-alloy and (b) NiSn-rGO-P3.3 composite.

The corrosion performance of the electrodeposited NiSn-P3.3 alloy and NiSn-rGO-P3.3 composite coatings was assessed by recording of the potentiodynamic polarization curves, as illustrated in Figure 5.19, and of the electrochemical impedance spectroscopy (EIS) spectra in aerated 0.5 M NaCl solution after different periods of immersion, up to 336 h, at room temperature. The composite material showed a slightly better corrosion performance as compared to pure NiSn alloy.

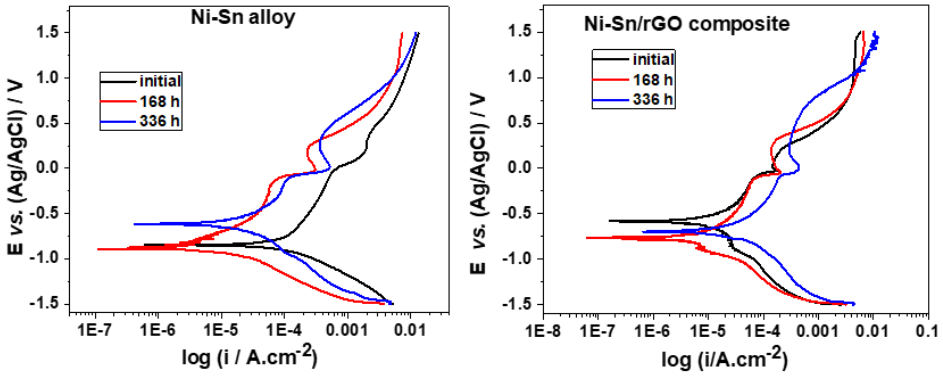

Figure 5.19. Polarization curves in semilogarithmic coordinates in 0.5 M NaCl for different periods of immersion (25 °C, 5 mV s^{-1}).

After 336 h of immersion in 0.5 M NaCl, the morphology of the sample was analyzed by SEM, as illustrated in Figure 5.21. The presence of a thin film is observed on top of both samples, evidencing a nano-petal like morphology, which may be ascribed to the formation of a nickel oxy-hydroxide layer. A similar morphology was reported in [54] for $Ni(OH)_2$ nanostructures formed as corrosion products on Ni nanofoams.

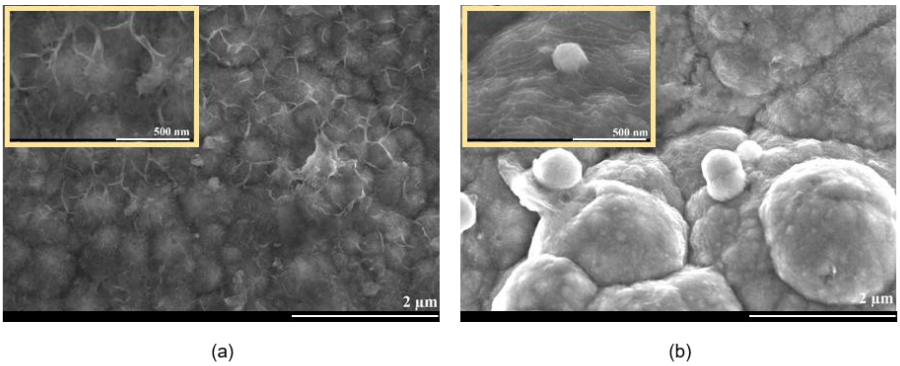

Figure 5.21. SEM SE micrographs of (a) NiSn-P3.3 alloy and (b) NiSn-rGO-P3.3 composite after 336h of immersion in 0.5 M NaCl.

The micro-mechanical properties of samples were investigated in cross-section. The incorporation of the carbon-based material into the metallic matrix does not influence the mechanical properties of the alloys. The hardness was found to be 8.21 ± 0.32 and 8.89 ± 0.68 GPa for the composite material and bare Ni-Sn alloy, respectively [55-57].

Chapter VI: Electrodeposition of ternary Sn-Cu-Ni alloys from deep eutectic solvents

The chapter presents several experimental results regarding the electrodeposition of Sn-Cu-Ni ternary alloys as an attractive lead-free solder candidate, involving deep eutectic solvents (DESs), namely using choline chloride-ethylene glycol and choline chloride-malonic acid eutectic mixtures. Prior to the electrodeposition process, the electrolyte has been characterized by cyclic voltammetry (CV) using GC working electrode in the choline chloride-malonic acid and choline chloride-etylene glycol eutectic mixtures containing $SnCl_2$, $CuCl_2$, $NiCl_2$ and ternary mixtures of $SnCl_2$+ $CuCl_2$+ $NiCl_2$ at 60 ^oC and different scan rates. The influence of the metallic ions concentration in the electrolyte has been investigated.

Different operation conditions have been applied to analyze the characteristics of the alloy coatings obtained by electrodeposition under DC from the two types of deep eutectic solvents from appearance, morphology, and composition viewpoints. In a first set of experiments, the bulk electrodeposition of Sn-Cu-Ni alloy onto Cu substrates has been performed involving electrolytes with the same concentrations of the metallic compounds (500 mM $SnCl_2{\cdot}2H_2O$ + 1.13 mM $NiCl_2{\cdot}6H_2O$ + 3.02 mM $CuCl_2{\cdot}2H_2O$) dissolved either in ILM or ILEG solvent (see Table 6.1).

The same values of the current density were applied, respectively of 5.33, 8, 10.67 and 13.33 mA cm^{-2}. Powdery, non-adherent alloy deposits have been obtained from choline chloride-malonic acid-based electrolytes for almost entire range of applied current density. The deposit detaches from the substrate and falls into the electrolyte. Instead, when using choline chloride-ethylene glycol eutectic mixture as solvent, adherent, uniform, and bright alloy coatings are deposited on the Cu substrate at current densities up to 8 mA cm^{-2}. As the current increased to 10.67 and 13.33 mA cm^{-2}, a dendritic growth occurred. The SEM micrographs are presented in Figures 6.9 and 6.10 respectively.

Table 6.1. The composition of choline chloride based ionic liquids containing metallic salts for Sn-Cu-Ni alloy electrodeposition.

System type	Deep eutectic solvent type/composition	Metallic compound, mmol dm^{-3}
ILM-1	Choline chloride–malonic acid, 1:1 (molar ratio) (ILM)	500 mM $SnCl_2 \cdot 2\,H_2O$ + 1.13 mM $NiCl_2 \cdot 6\,H_2O$ + 3.02 mM $CuCl_2 \cdot 2\,H_2O$
ILEG-1	Choline chloride–ethylene glycol, 1:2 (molar ratio) (ILEG)	500 mM $SnCl_2 \cdot 2\,H_2O$ + 1.13 mM $NiCl_2 \cdot 6\,H_2O$ + 3.02 mM $CuCl_2 \cdot 2\,H_2O$
ILEG-2		500 mM $SnCl_2 \cdot 2\,H_2O$ + 0.25 mM $NiCl_2 \cdot 6\,H_2O$ + 0.685 mM $CuCl_2 \cdot 2\,H_2O$
ILEG-3		500 mM $SnCl_2 \cdot 2\,H_2O$ + 0.055 mM $NiCl_2 \cdot 6\,H_2O$ + 0.345 mM $CuCl_2 \cdot 2\,H_2O$

Since the quality of the Sn-Cu-Ni alloy coatings electrochemically prepared in ILEG based electrolyte showed proper characteristics from appearance, adhesion and homogeneity viewpoints, the further experiments have been performed involving this type of eutectic mixture.

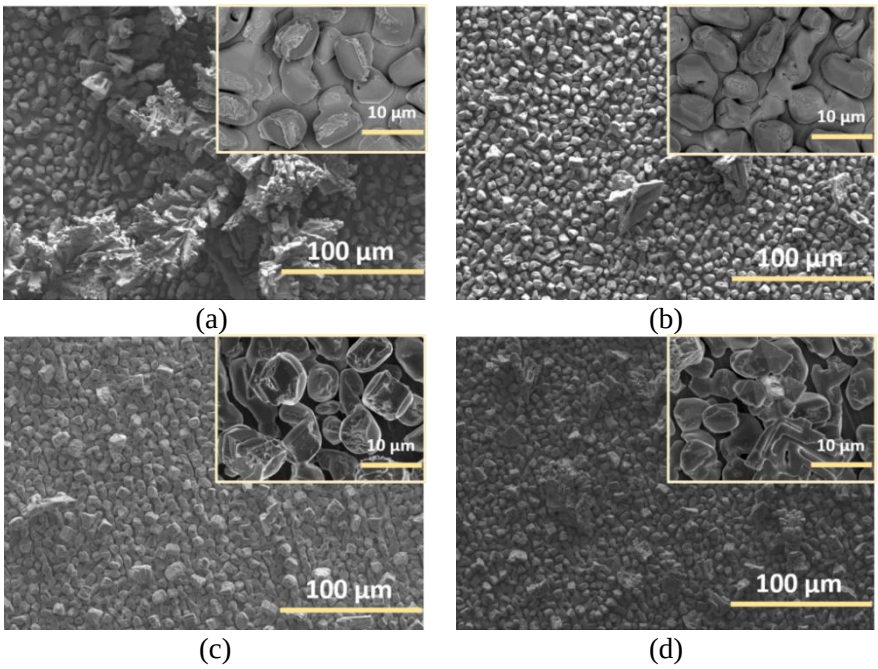

Figure 6.9. SEM micrographs of Sn-Cu-Ni alloy electrodeposited from ILM-1 (500 mM $SnCl_2 \cdot 2H_2O$ + 1.13 mM $NiCl_2 \cdot 6H_2O$ + 3.02 mM $CuCl_2 \cdot 2H_2O$ in ILM) at: (a) 5.33; (b) 8; (c) 10.67 and (d) 13.33 mA cm^{-2} (60 ^oC, 30 min.).

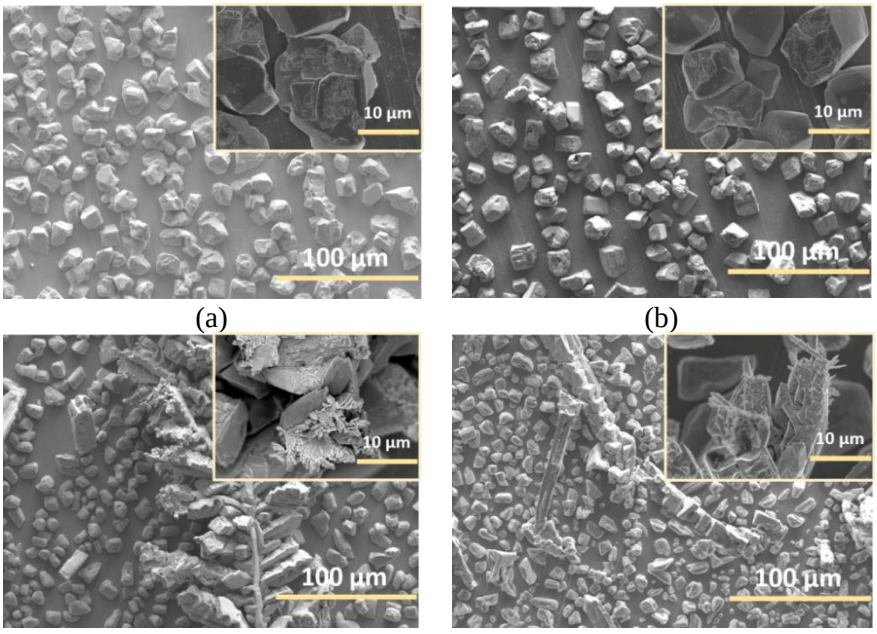

Figure 6.10. SEM micrographs of Sn-Cu-Ni alloy electrodeposited from ILEG-1 (500 mM $SnCl_2 \cdot 2H_2O$ + 1.13 mM $NiCl_2 \cdot 6H_2O$ + 3.02 mM $CuCl_2 \cdot 2H_2O$ in ILEG) at: (a) 5.33; (b) 8; (c) 10.67 and (d) 13.33 mA cm^{-2} (60 °C, 30 min.).

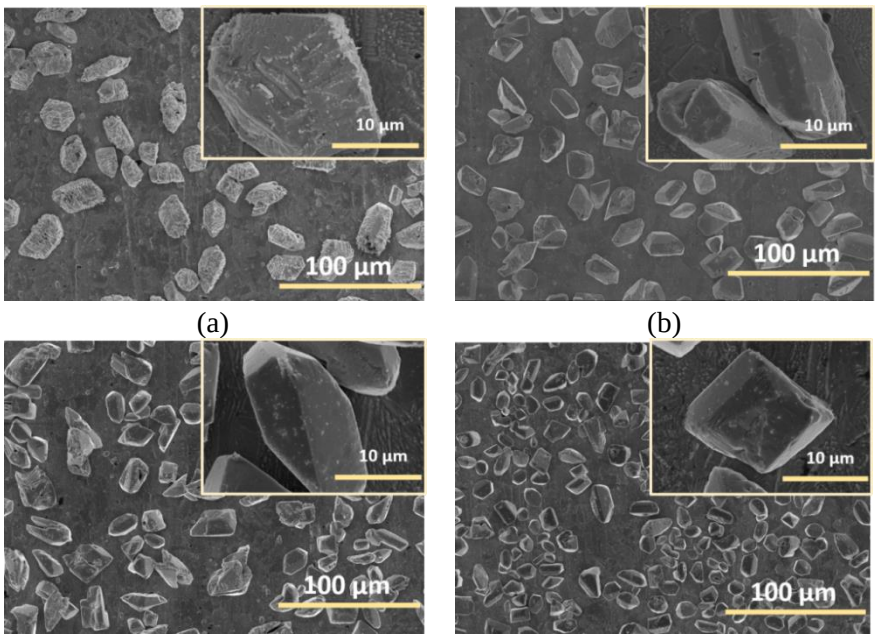

Figure 6.13. SEM micrographs of direct current electrodeposition of Sn-Ni-Cu alloys from ILEG-3 (500 mM $SnCl_2 \cdot 2H_2O$ + 0.055 mM $NiCl_2 \cdot 6\ H_2O$ + 0.345 mM $CuCl_2 \cdot 2\ H_2O$) at: (a) 5.33 mA/cm^2; (b) 8 mA/cm^2; (c) 10.67 mA/cm^2 and (d) 13.33 mA/cm^2.

As a second objective of this investigation is to achieve ternary Sn-Cu-Ni alloy coatings having a composition close to Sn-0.7Cu-0.05Ni solder with the eutectic or near eutectic melting temperature of about 227 ºC [13,14,78,79], suitable for electronic industry applications. Various electrolyte formulations containing different concentrations of Ni and Cu compounds in choline chloride-ethylene glycol eutectic mixture have been tested. In addition, a particular attention was given to the Ni content in the solder alloy due to its very low recommended concentration. According to EDX analysis, a $[Ni^{2+}]/[Cu^{2+}]$ molar ratio of

0.16 produced a Sn-Cu-Ni alloy containing 99.29 wt.% Sn, 0.65 wt.% Cu and 0.06 wt.% Ni at the optimum driven current density of 8 mA cm^{-2}, quite close to the industrial Sn-0.7Cu-0.05Ni solder composition. Figure 6.13 illustrates the SEM micrographs of the Sn-Cu-Ni alloy coating electrodeposited at different current densities.

XRD analysis has been applied to get information on the present phases in the electrodeposited Sn-Cu-Ni ternary alloy films. Besides the peaks corresponding to the copper substrate (card No. 00-004-0836), the peaks for tetragonal tin (card No.00-004-0673), monoclinic Cu_6Sn_5 (card No.: 01-076-2703) and cubic $CuNi_2Sn$ (ICSD#103068) intermetallics have been identified [67,80,81]. Compared to the Sn standard pattern, a preferred orientation growth to (200), peak at 30.43 º was noticed for the alloy deposit.

TGA analysis has been performed to measure the melting point of the electrodeposited Sn-Cu-Ni ternary alloy. A melting point of 229 ºC has been determined, as seen in Figure 6.17, quite close to the values reported in the literature for Sn-Cu-Ni alloy solders with different concentrations of Cu and Ni, in the range of 226-232.2 ºC [82,83].

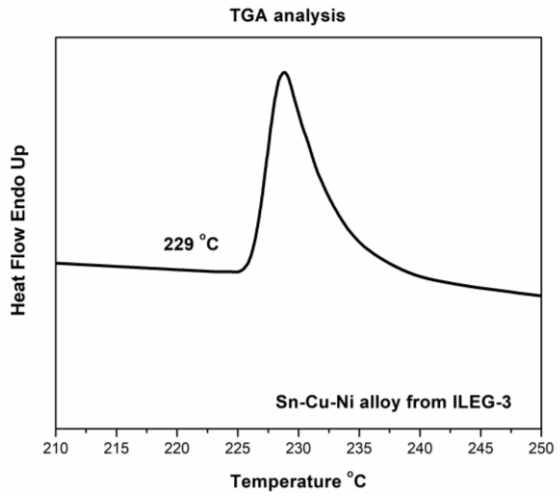

Figure 6.17. TGA analysis for Sn-Cu-Ni alloy electrodeposited from ILEG-3 system (500 mM $SnCl_2{\cdot}2H_2O$ + 0.055 mM $NiCl_2{\cdot}6H_2O$ + 0.345 mM $CuCl_2{\cdot}2H_2O$ in ILEG) at 60 °C for 30 min, 8 mA cm^{-2} (Ti substrate).

In terms of corrosion protection of electronic equipment, the electrochemical behavior of Sn-Ni-Cu alloy coatings was evaluated by potentiodynamic polarization and electrochemical impedance spectroscopy (EIS) in 0.5 M NaCl aqueous solution at room temperature (Figure 6.18). A typical polarization plot in semilogarithmic coordinates corresponding to the as-deposited Sn-Cu-Ni alloy (99.29 wt.% Sn, 0.65 wt.% Cu and 0.06 wt.% Ni) coating is presented in Figure 6.18 (a).

The corrosion current density, i_{corr} and corrosion potential, E_{corr}, were determined by Tafel extrapolation of both cathodic and anodic branches of polarization curve. E_{corr} was measured at around -0.627 V vs. Ag/AgCl, while the value of i_{corr} was 6.8 µAcm^{-2}. It appeared that the Sn-Cu-Ni ternary alloy coatings exhibit a better corrosion performance as compared to Sn-Ni alloys electrodeposited from ILEG based electrolytes, with at least one order of magnitude lower corrosion current density [46,72]. Moreover, the determined corrosion current value is slightly lower as compared to 8.98 µAcm^{-2} that was reported in [84] for Sn-0.7Cu-0.05Ni lead-free solder.

The electrochemical impedance spectra of Sn-Cu-Ni alloy coating recorded at open circuit potential (OCP) in 0.5 M NaCl are illustrated in Figure 6.18 (b) and (c) as Bode and Nyquist plots. The Nyquist diagram presents a semicircle arc in the relatively high-frequency range and its diameter is associated with the polarization resistance which may be correlated to the rate of corrosion. Bode plot shows the value of phase angle maximum at around -60º meaning less electrically insulating products.

The equivalent circuit (EC) used to describe corrosion behavior of Sn-Cu-Ni alloy deposits in the NaCl solution is shown in the inset of Figure 6.18 (c). It consists in an ohmic resistance of solution (Rs) in series to a complex parallel circuit. In this circuit, a double-layer capacitor (Cdl) is in parallel with a charge-transfer resistor (R_{CT}) in series with a second circuit containing a film capacitor (C_F) in parallel with a film resistor (R_F). To fit the experimental data, constant phase elements (CPE) have been used instead of true capacitances [85,86, 87]. The values of circuit parameters which are obtained by fitting the impedance data with Zview software using the proposed EC.

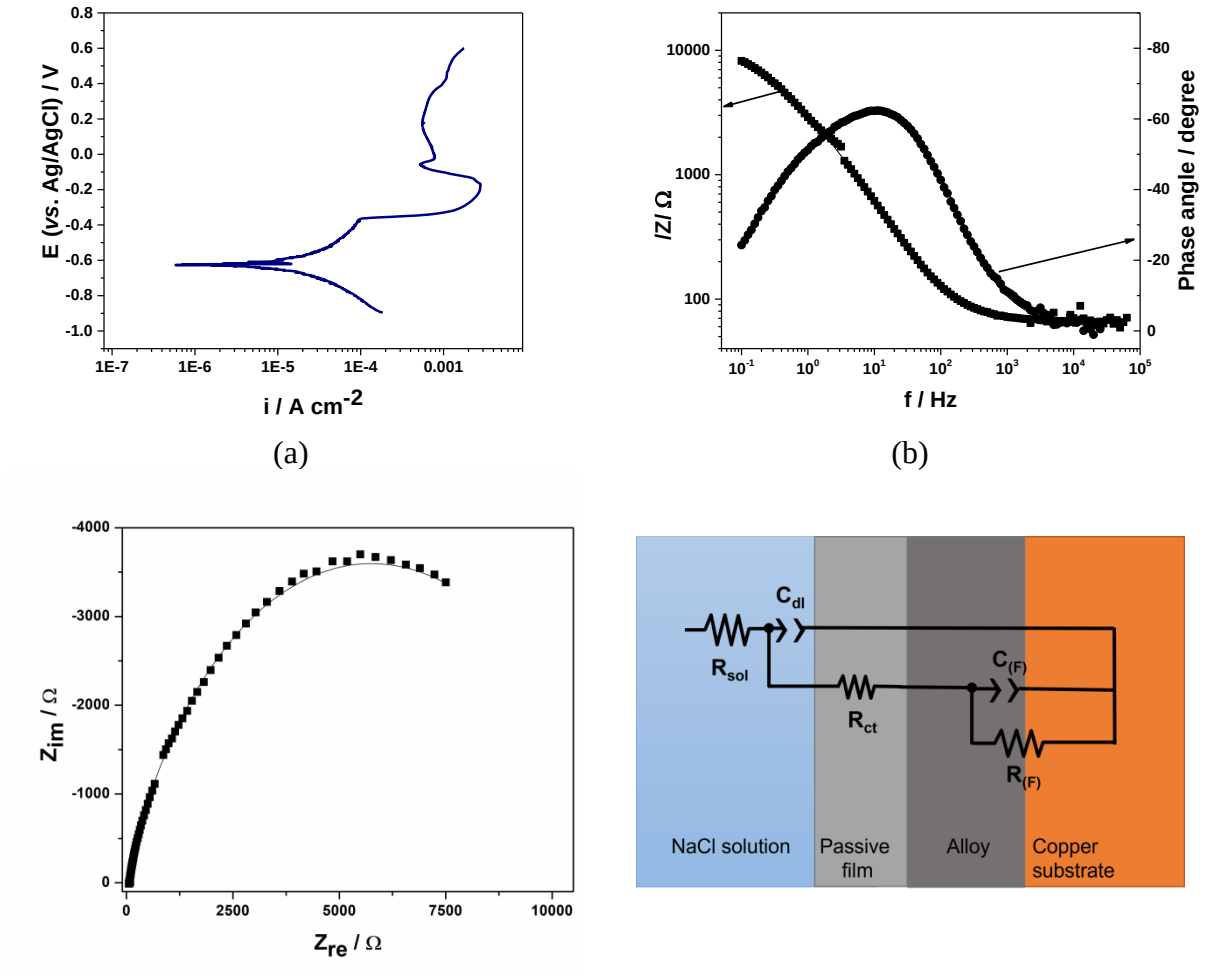

Figure 6.18. Corrosion behavior of Sn-Cu-Ni alloy coating in 0.5 M NaCl: (a) polarization curve in semilogarithmic coordinates (25 ^{o}C, 3 mV s^{-1}); (b) Bode plot and (c) Nyquist plots at open circuit potential (solid lines are the fit to the measured points using the equivalent circuit presented in (d).

Chapter VII: Corrosion behavior of Sn-Cu-Ni lead-free solders from deep eutectic solvents

In the previous chapter we have optimized the content of the metallic salts in the ILEG deep eutectic solvent in order to obtain Sn-Cu-Ni alloy coatings with a composition close to the reported industrially for Sn-0.7Cu-0.05Ni solder. In this chapter we report our studies in the same electrolyte changing the galvanostatic conditions through the use of either direct current or pulsed current modes at different applied frequencies (see Table 7.2).

Table 7.2. Operating parameters for the electrodeposition of Sn-Ni-Cu alloys from ILEG based electrolyte.

	SnCuNi-DC	***SnCuNi-P1***	***SnCuNi-P2***	***SnCuNi-P3***	***SnCuNi-P4***
On- and Off- time duration of the pulse	-	T_{ON}= 10 ms T_{OFF} = 50 ms	T_{ON}= 100 ms T_{OFF} = 500 ms	T_{ON}= 1 s T_{OFF} = 5s	T_{ON}= 10 s T_{OFF} = 50 s
Frequency (Hz)	-	f = 16.67	f = 1.67	f = 0.167	f = 0.0167
Duty cycle (%)	-	θ = 16.7	θ = 16.7	θ = 16.7	θ = 16.7
Current density (mA/cm²)	i= 8	i_{av} = 8	i_{av} = 8	i_{av} = 8	i_{av} = 8

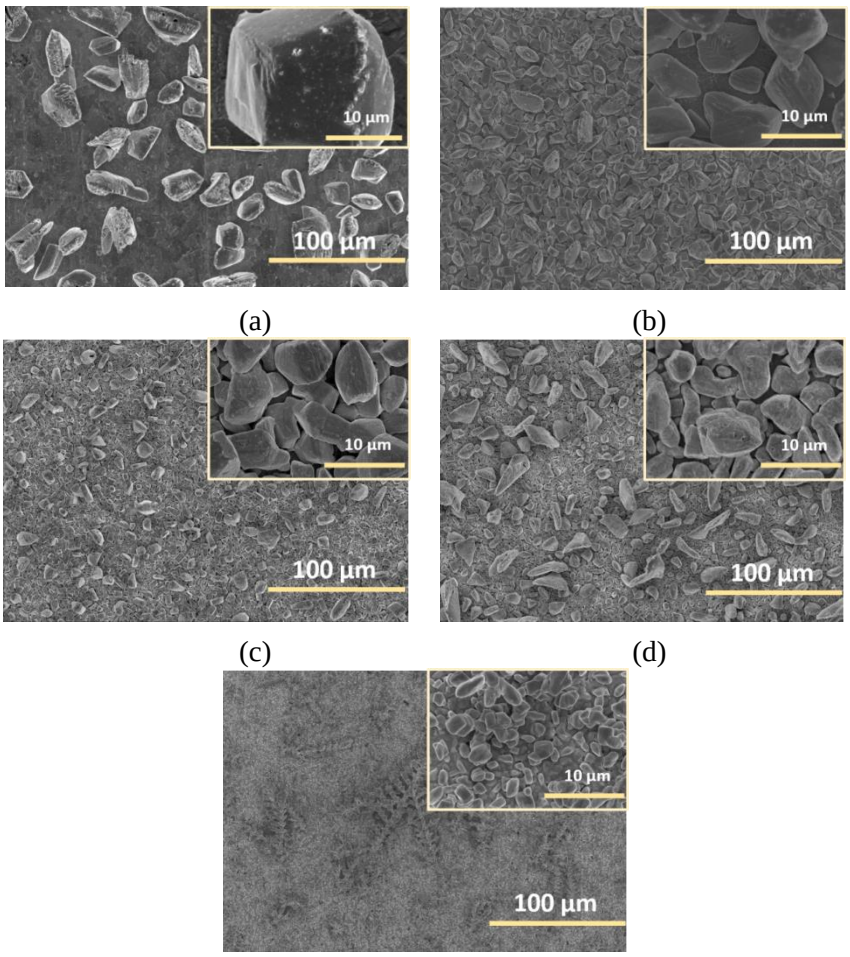

Figure 7.2. SEM micrographs of Sn-Cu-Ni alloys: (a) SnCuNi-DC; (b) SnCuNi-P1; (c) SnCuNi-P2; (d) SnCuNi-P3 and (e) SnCuNi-P4.

Figure 7.2 shows the surface morphology of the Sn-Cu-Ni alloys coatings electrodeposited on copper substrates from ILEG deep eutectic solvent containing 500 mM $SnCl_2$, 0.055 mM $NiCl_2$ and 0.345 mM $CuCl_2$. Under DC conditions at 8 mA/cm^2 large irregular grains are observed in SEM images (Figure 7.2a). It can be seen from Figure 7.2b-e the deposit compactness is improved with decreasing the applied frequency and a diminution in the grain size is detected. By analysing SEM images (both on the sample surface and as cross-section) we determined that the grain size of the Sn-Cu-Ni alloy prepared under DC

electrodeposition conditions was larger (values of 16.7±4.1 µm) than of the samples obtained with pulse plating (7.4 ±2.4, 4.3± 1.7, 3.1±1.2 and 1.4±0.5 µm for SnCuNi-P1, SnCuNi-P2, SnCuNi-P3 and SnCuNi-P4, respectively). The effect of the DC and PC electrodeposition conditions on the chemical content and melting point of Sn-Cu-Ni alloys was studied by elemental analysis and DSC on powdery samples. It is clearly observed that both copper and nickel content in Sn-Cu-Ni alloys increased when PC electrodeposition is used.

Figure 7.7 presents the DSC curves. The DSC data showed that the changes observed in the alloy composition influence the melting temperature. Only a single endothermic peak can be observed in Figure 7.7 for DSC curves of each sample composition. The use of pulsed current lead to a decrease in the melting temperature.

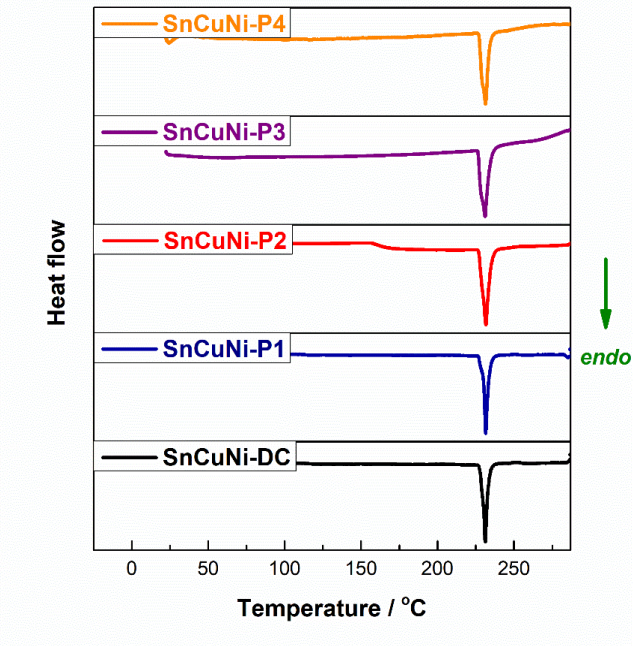

Figure 7.7. Differential scanning calorimetry (DSC) analysis of the Sn-Ni-Cu alloys obtained under direct current (SnNiCu-DC) and pulse current electrodeposition conditions: SnCuNi-P1, SnCuNi-P2, SnCuNi-P3, and SnCuNi-P4.

We continued investigations in detail of EDS elemental analysis and corrosion studies only for SnCuNi-DC and SnCuNi-P2. We selected SnCuNi-P2, which will be named the PC sample as a representative for pulsed current electrodeposition, since its morphology is very different from the sample prepared under DC and SnCuNi-P1 system. The melting temperature of SnCuNi-P2 is lower compared to DC sample and the corresponding current efficiency is not too low as for the samples SnCuNi-P3 and SnCuNi-P4 synthetized at very low applied pulse frequency.

Figure 7.13 presents the corrosion behavior characterization of SnCuNi-DC and SnCuNi-P2 samples using two electrochemical techniques: potentiodynamic polarization and EIS (Nyquist curves). Data regarding corrosion potential and corrosion current were determined graphically from polarization curves at the intercept of the anodic and cathodic Tafel lines. The obtained values of corrosion potentials for both samples were quite similar, at almost -0.62 V *vs* Ag/AgCl, although the corrosion current was lower for the sample prepared by PC (2.6 µA/cm^2) than for the sample prepared by DC (6.8 µA/cm^2). The cathodic branches of polarization for both samples represent the usual electroreduction of dissolved oxygen molecules in a neutral aqueous solution of NaCl, leading to increment of pH due to the formation of OH^- anions [26].

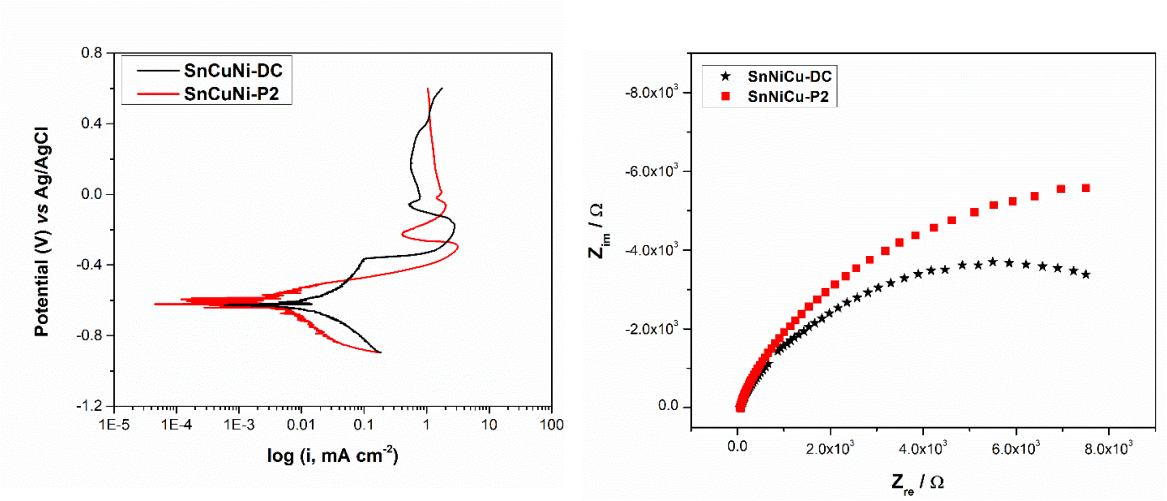

(a) (b)

Figure 7.13. Corrosion investigations on SnCuNi-DC and SnCuNi-P2: (a) potentiodynamic polarization curves and (b) electrochemical impedance spectroscopy (Nyquist plot).

Figure 7.13-b shows in the entire frequency region the Nyquist semicircles of which diameters represent polarization resistance R_p, a parameter which is inversely proportional to corrosion current. It is clear that the larger diameter of curve for sample prepared in pulse means a lower corrosion current than for sample prepared in DC, confirming the data from polarization curves. Also, the lack of any supplementary straight line following the semicircle demonstrates that the formed passive films are not stable.

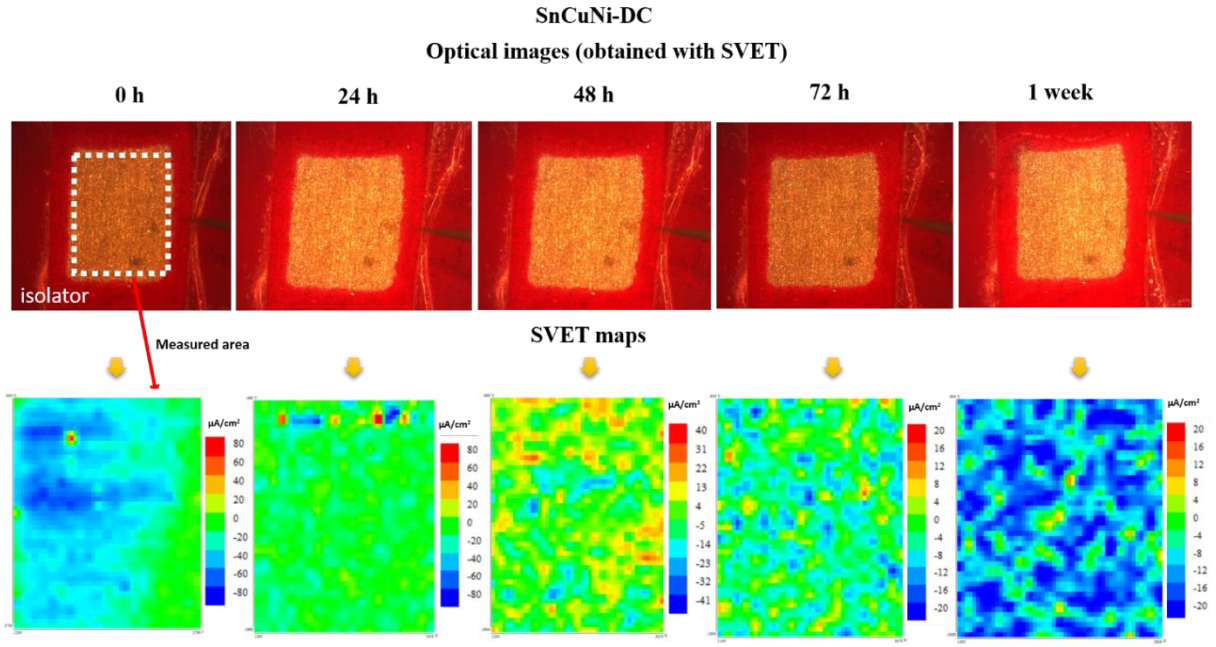

Figure 7.14. SVET measurement on the sample prepared under direct current electrodeposition conditions (SnCuNi-DC) over 1-week immersion in 0.1 M NaCl solution: (a) optical image before SVET analysis and (b) current density mapping.

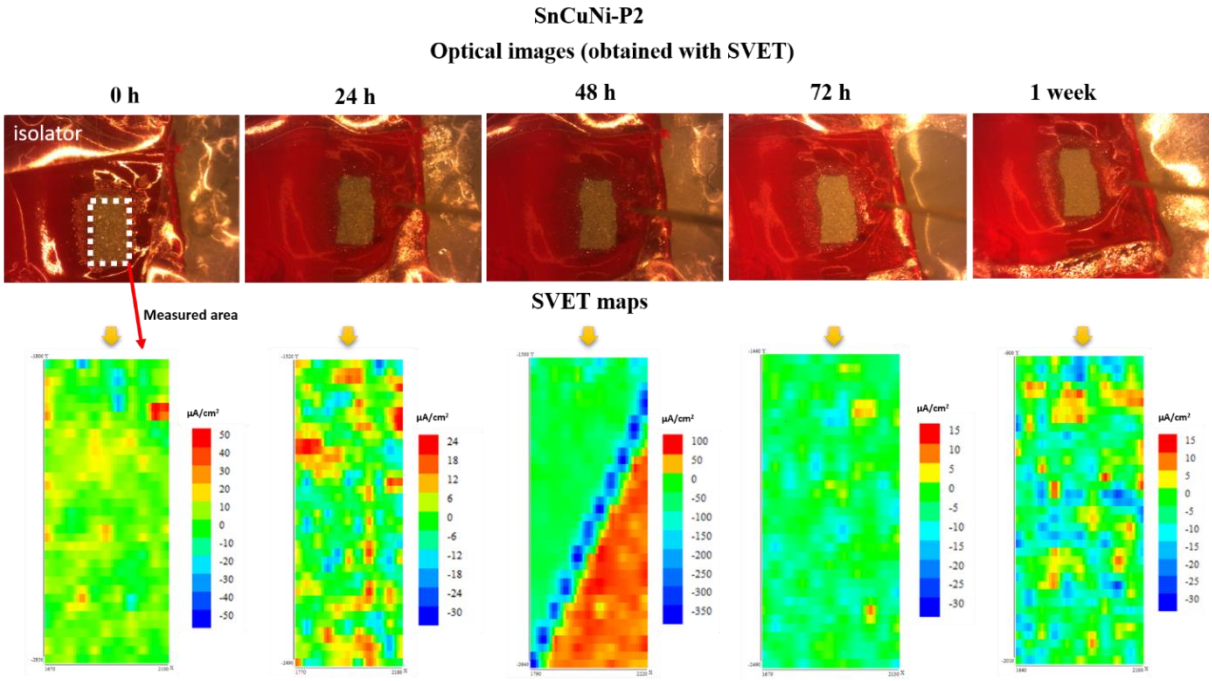

Figure 7.15. SVET measurement on the SnCuNi-P2 sample prepared under pulsed current electrodeposition conditions over 1-week immersion in 0.1 M NaCl solution: (a) optical image before SVET analysis and (b) current density mapping.

Figure 7.14 and 7.15 exhibit the optical microscopy images and ionic the current density maps obtained by using the scanning vibrating electrode technique (SVET) of the representative samples: SnCuNi-DC and SnCuNi-P2. The samples were immersed in 0.1 M NaCl aqueous electrolyte over 1-week and the current density maps were recorded every 24 h (every day). SVET provides insight into the localized processes of corrosion, providing information about the corrosion behavior of the coating on a microscopic scale. Investigation showed the presence of anodic and cathodic activities on the surface (positive and negative current values represented with red and blue colors respectively). The anodic activity is associated with the dissolution of the metallic grains, mainly tin. The cathodic current is due to electroreduction reaction of dissolved oxygen in the neutral aqueous solution [28]. The corrosion products mainly consist of tin oxide and hydroxide species. A noticeable difference is observed between samples at everyday immersion.

From the SVET experiments after 1-week immersion (Figure 7.14 and 7.15), it can be seen that both samples prepared by DC and PC showed a decrease in the anodic current density determined by SVET, indicating the possible formation of a passive film on the samples surface. This is confirmed by SEM and EDX analysis of samples after 1-week immersion in 0.1 M NaCl, as shown in Figure 7.16. The corrosion products were investigated by Raman spectroscopy after 1-week immersion. Analyzing the raman spectra and considering the literature data, the peaks at 184, 227 and 264 cm^{-1} are attributed to the complex tin oxi-hydroxychloride $Sn^{II}_3O_2(OH)_{2-x}Cl_x$ ($0<x<1$) while the peak at 131 cm^{-1} may be assigned to a transition oxide phase SnO_x ($1<x<2$) [30-32]. However, on the SnCuNi-P2 sample, an additional Raman broad signal is detected in a range from 470-680 cm^{-1} which could be attributed to the formation of amorphous $Sn^{IV}O_2$ [31].

Based on the results obtained a reaction path for the formation of the corrosion products is showed in Figure 7.23 together with a schematic of a proposed mechanism for the PC and DC systems. Tin as the main constituent from the solder alloy will act as the anode in the galvanic coupling having a lower corrosion potential than that of the Cu substrate, which acts as the cathode. The reactions on the anode are complicated. Tin ions will react with the hydroxide ions generated from the oxygen reduction reaction at the cathode leading to the

formation of tin hydroxide species. The presence of chloride ions in the solution transforms the hydroxide species into $Sn_3O_2(OH)_{2-x}Cl_x$ phase followed by its conversion into tin oxide compounds [31-33]. $Sn^{IV}O_2$ as the final corrosion product is observed just on the sample prepared under PC.

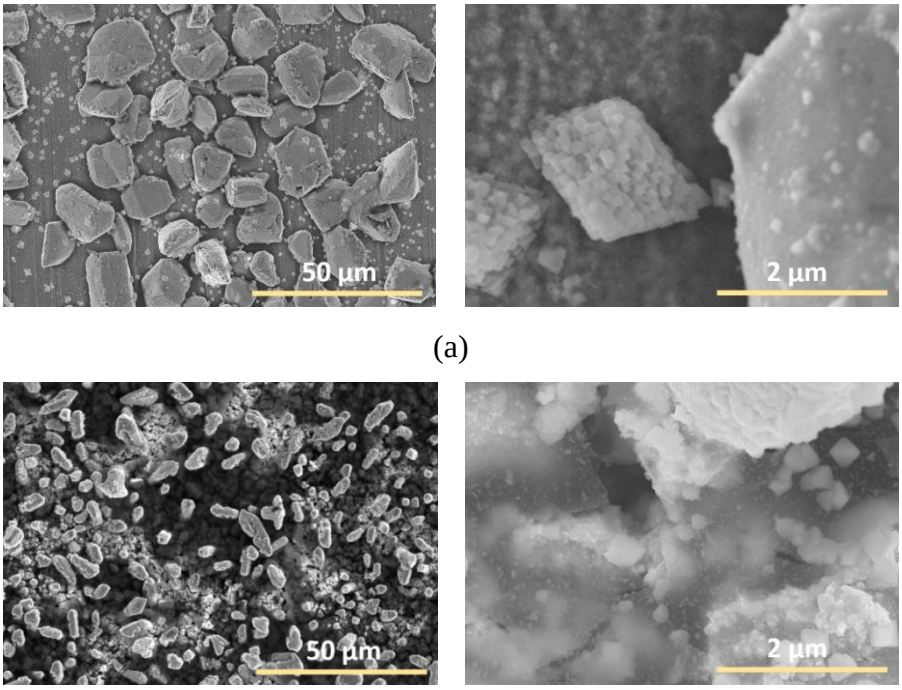

Figure 7.16. SEM micrographs on compared samples: (a) SnCuNi-DC and (b) SnNiCu-P2 after one-week immersion in 0.1 M NaCl solution.

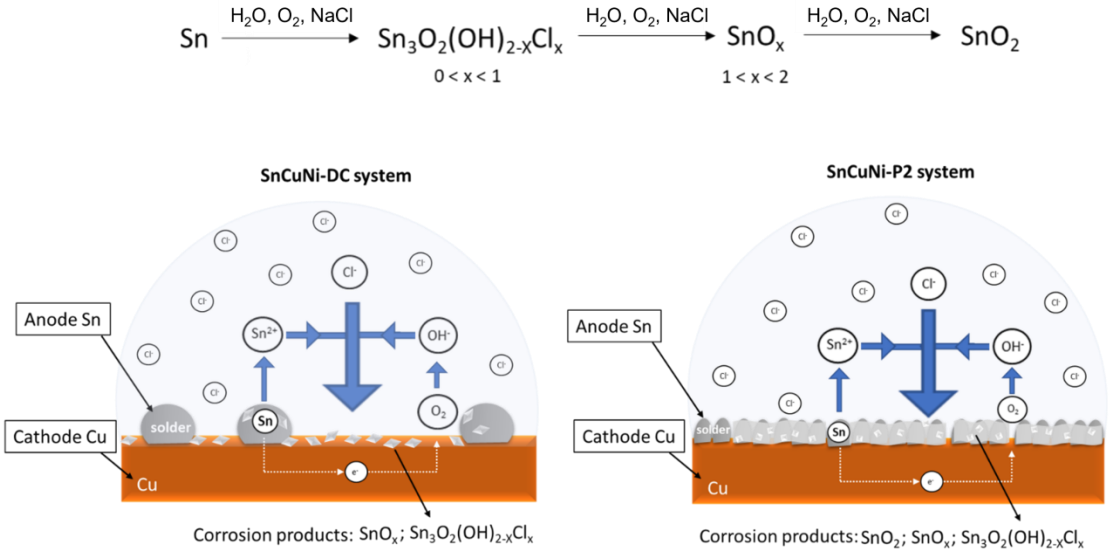

Figure 7.23. Reaction and schematic illustration of the corrosion mechanism of SnCuNi-DC and SnCuNi-P2 system in NaCl.

Chapter VIII: Scale-up electrodeposition of Sn-Cu-Ni alloy on PCBs from deep eutectic solvents and industrial reflowing

In this chapter we present a description of the pilot plant setup and its use in the deposition of Sn-Cu-Ni alloy from deep eutectic solvent based on choline chloride: ethylene glycol mixture under direct current (DC) and pulsed current (PC) mode.

Electrodeposition of Sn-Cu-Ni alloys was scaled-up on an existing pilot plant as is illustrated in Figure 8.2. The pilot plant consists of a cleaning surface tank, a water rinse after cleaning tank, a micro-etching tank, a water rinsing after micro-etching, an alcohol rinse tank, an electroplating tank, an ionic liquid rinse tank and a final water rinse tank.

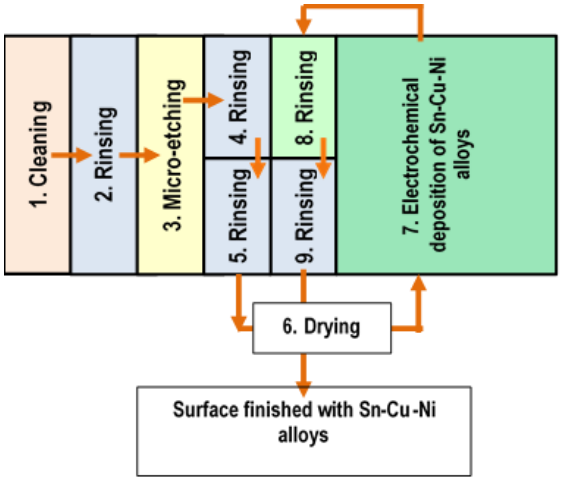

Figure 8.2. Follow diagram of the electrodeposition process of Sn-Cu-Ni alloys from DESs in the pilot plant.

Regarding the electrodeposition process, the composition of the electrolyte was previously established from the investigation carried (500 mM $SnCl_2 \cdot 2H_2O$ + 0.345 mM $CuCl_2 \cdot 2H_2O$ + 0.055 mM $NiCl_2 \cdot 6H_2O$) out at lab-scale. Sn-Cu-Ni alloys are deposited under direct current (i= 8 mA/cm^2) and pulse current mode (f=1.67 Hz).

In order to test the potential of Deep Eutectic Solvents electrolytes as substitutes for dangerous and costly processes applied on the manufacturing of Printed Circuit Boards, Sn-Cu-Ni alloys were electrodeposited into PCBs from the prototype bath to act as etch resist and solder base for components soldering on the board. The printed circuit boards (PCB) tested are illustrated in Figure 8.7.

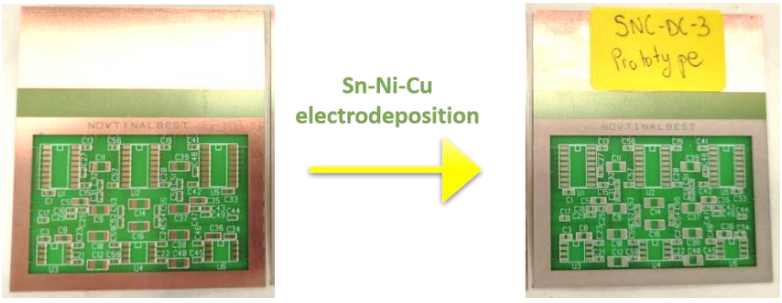

Figure 8.7. Printed circuit board (PCB) before and after electrodeposition of Sn-Cu-Ni alloy on pilot plant.

Panels covered with copper finish were plated with Sn-Cu-Ni alloy under direct and pulsed current mode. Each board has pads with different dimensions. SEM micrographs of the surface of the rectangular pad 'U2' (surface pad:1.14 x 1.8 mm^2) are reported in Figure 8.8 and 8.9.

No variation in the morphology of the coating was observed among the pads. Under DC, more dendrite are detected at the margin of the pads caused by an increase in the current density at the edges as compared to the centre of the deposited surface [14]. The use of pulse current decreases the dendrite formation.

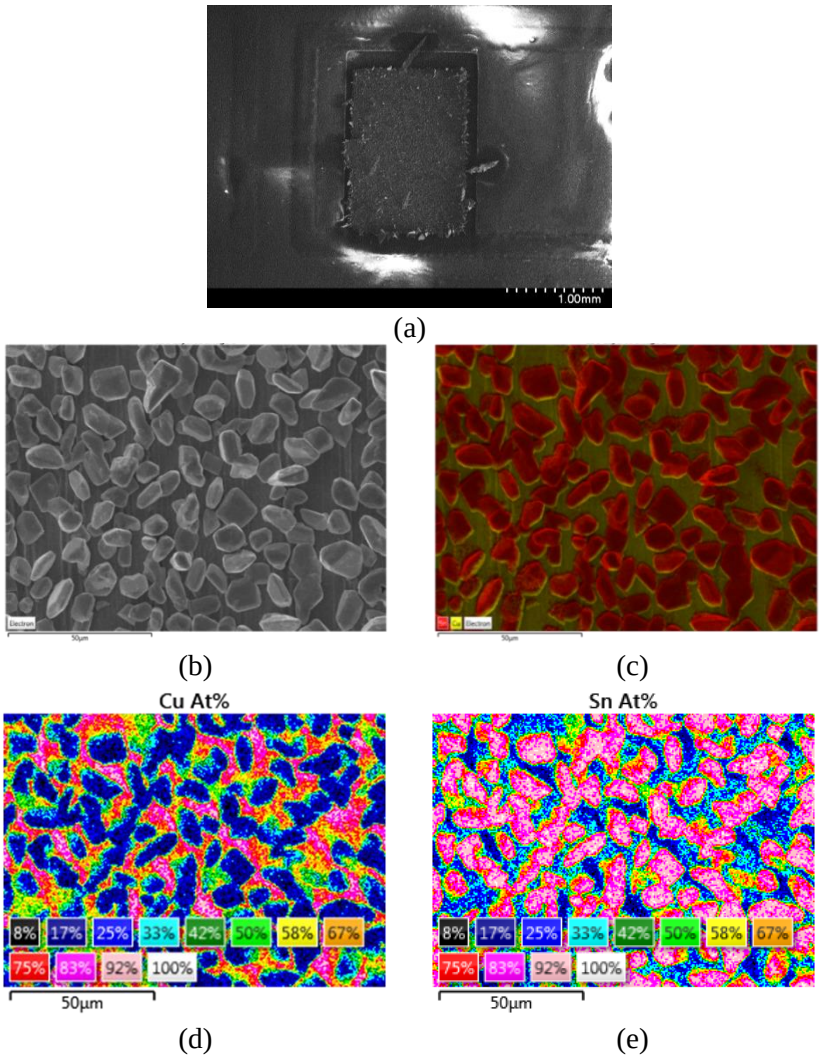

Figure 8.8. Sn-Cu-Ni alloy electrodeposited on a PCB pad from prototype bath at 8 mA/cm^2 (a) and (b) SEM micrograph at different magnifications (c) EDX qualitative map at with Sn element represented in red and copper in yellow and (d), (f) are the EDX quantitative maps for Cu and Sn respectively in atomic percentage.

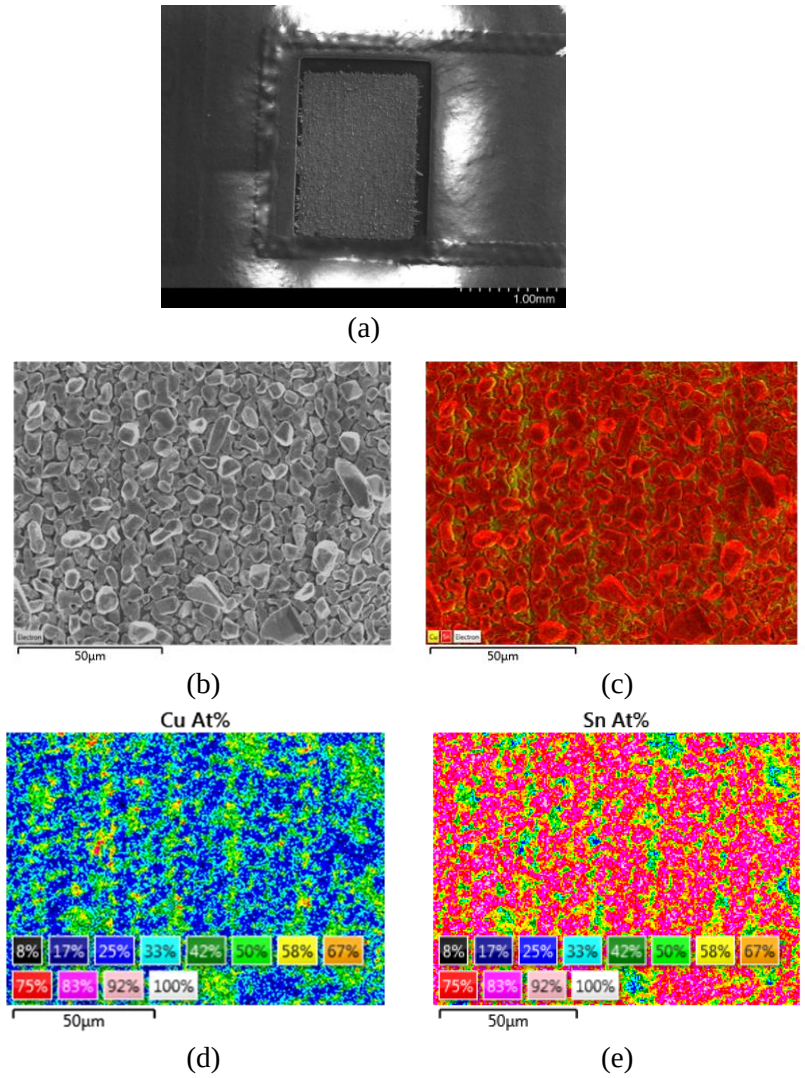

Figure 8.9. Sn-Cu-Ni alloys electrodeposited on copper foil using pilot plant under PC mode (T_{on}= 100 ms, T_{off} = 500 ms, f=1.67 Hz) at 8 mA/cm^2 (a) and (b) SEM micrograph (c) EDX qualitative analysis with tin represented in red and copper in yellow and (d),(e) are EDX quantitative maps representing the atomic percentage distribution of copper and tin respectively.

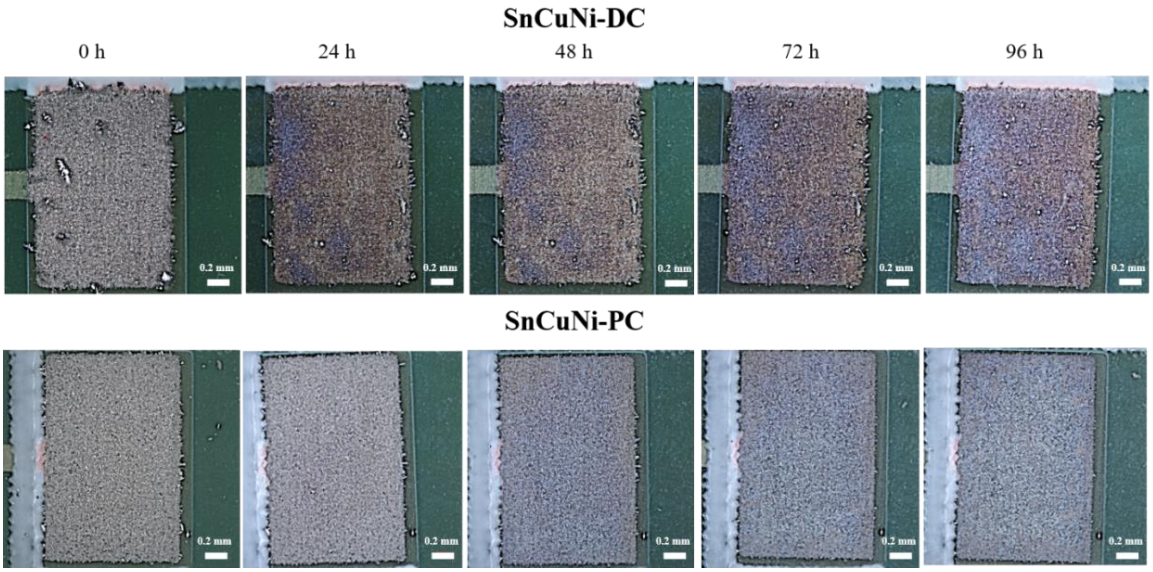

Figure 8.11. Appearance of PCBs (U2-left pad) covered with Sn-Cu-Ni alloy under direct current and pulsed current after salt spray test.

Printed circuit boards covered with Sn-Cu-Ni alloy coating realized using the pilot plant under direct current (SnCuNi-DC) and pulsed current (SnCuNi-PC) mode have been exposed to the salt spray cabinet in order to simulate a corrosive attack in a harsh environment during 96 h. The samples were investigated every 24 h using an optical microscope and the results are showed in Figure 8.11.

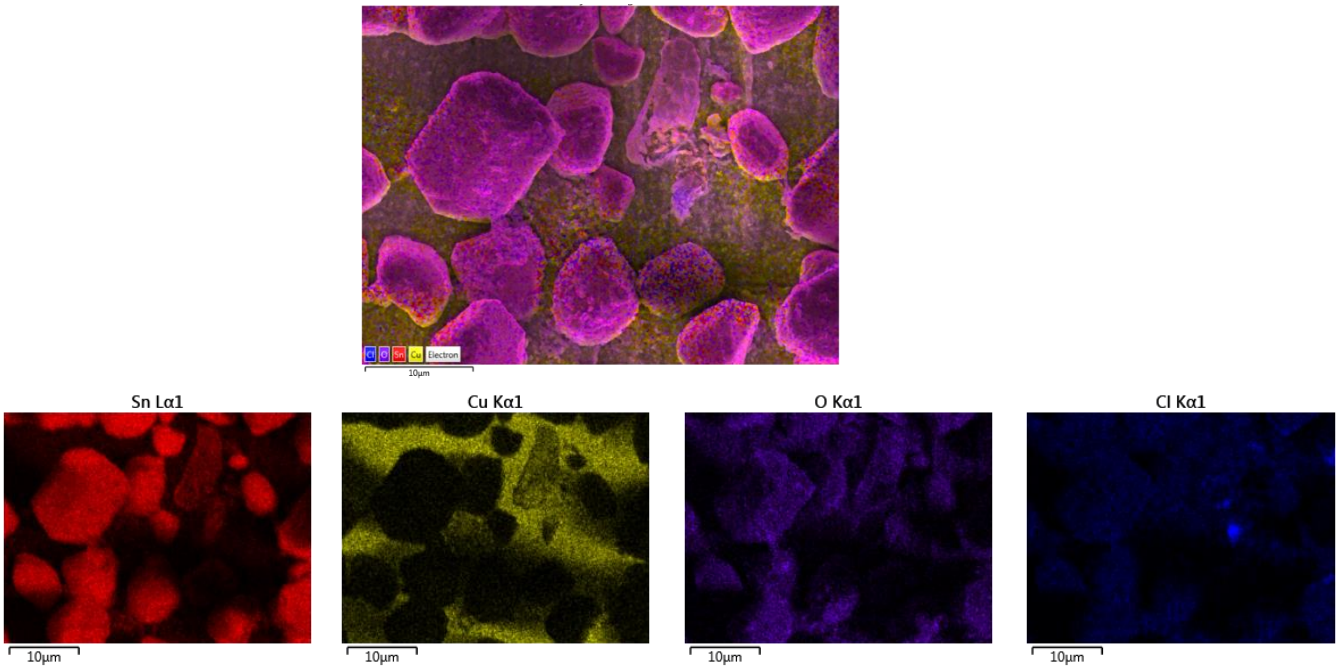

Figure 8.3. EDX qualitative analysis map of SnCuNi-DC alloy electrodeposited on a PCB pad from prototype bath under DC mode at 8 mA/cm^2 after 96 h of exposure to Salt Spray test.

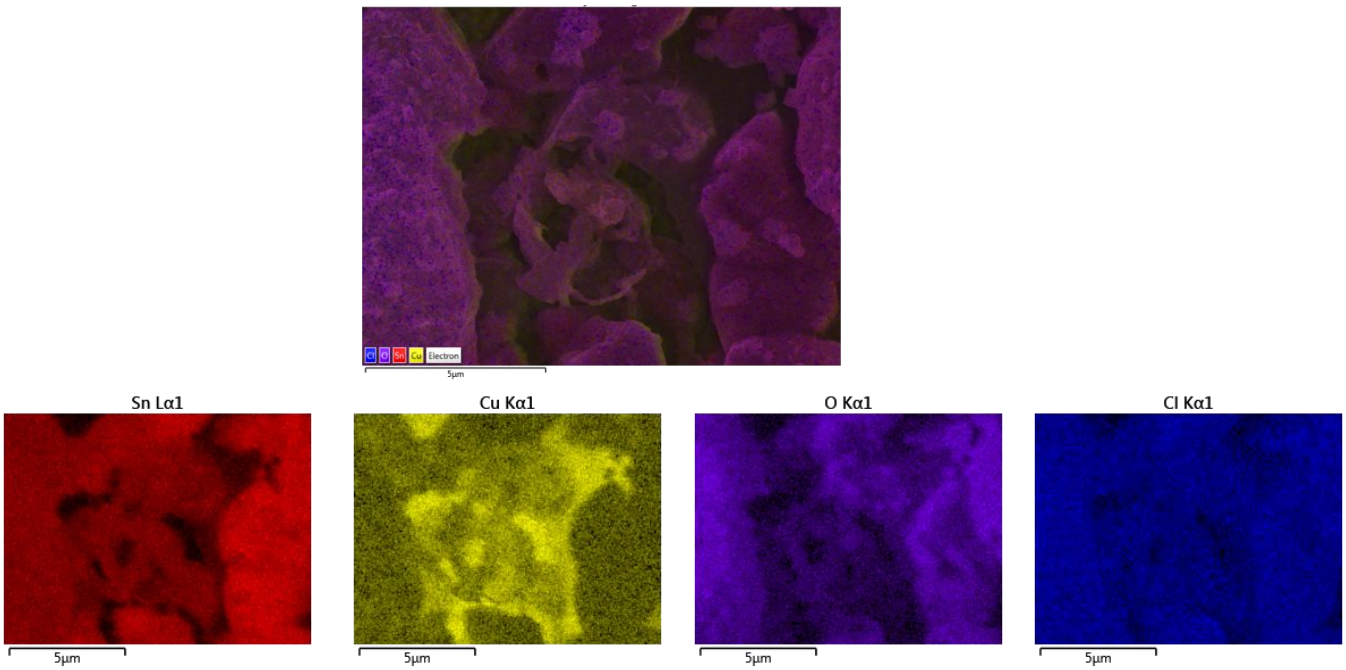

Figure 8.17. EDX qualitative analysis map of SnCuNi-PC alloy electrodeposited on a PCB pad from prototype bath under PC mode (Ton= 100 ms, Toff = 500 ms, f=1.67 Hz) at 8 mA/cm^2 after 96 h of exposure to Salt Spray test.

It is evident that the samples coated with Sn-Cu-Ni alloy under direct current conditions show high signs of corrosion attack, even after 24 h of exposure. However, on the

PCBs coated under pulse current (SnCuNi-PC) the corrosion attack is observed later, after 48 h. Furthermore, even after 96 h the coated exhibited good corrosion resistance.

The SEM-EDX micrograph of the samples after 96 h of exposure to saline environment are showed in Figure 8.3 and 8.17 for DC and PC systems respectively. For DC plating mode, part of the grains was affected by the corrosive media; however, the copper substrate looks unchanged. In the case of the PCBs covered with Sn-Cu-Ni alloy obtained under pulse current plating mode, the corrosion process involves the formation of a passive film that partially cover the surface of the sample as seen in Figure 8.17.

Effect of reflowing into the properties of Sn-Cu-Ni alloy from deep eutectic solvent

After the PCBs are design and covered with the suitable finish, they are sent to a manufacturing company where electronic components are mounted on their surface in order to fulfil its function. Mibatron S.R.L. (https://www.mibatron.ro/) is a Romanian company experienced in PCB assembly with more than 25 years in the industry. It is specialized in automated PCB assembly for both surface mound and through hole technology. In order to determine how the reflowing process will affect the Sn-Cu-Ni alloy coatings, copper sheets (s=7.5 cm^2) coated with the alloy under direct current (SnCuNi-DC) and pulsed current (SnCuNi-PC) were exposed to the reflow process in the industrial oven at MIBATRON S.R.L. company. The temperature in the oven is gradually increased from 160 ºC to 260 ºC during ~ 7 min. After reflowing the grains are partially melted. The exposure to the reflowing process induces a change in the composition of the alloy as it could be seen in the EDX quantitative analysis (see Figures 8.23 and 8.24) and the grains become richer in copper. This phenomenon is a result of the diffusion of the copper from the substrate into the grains.

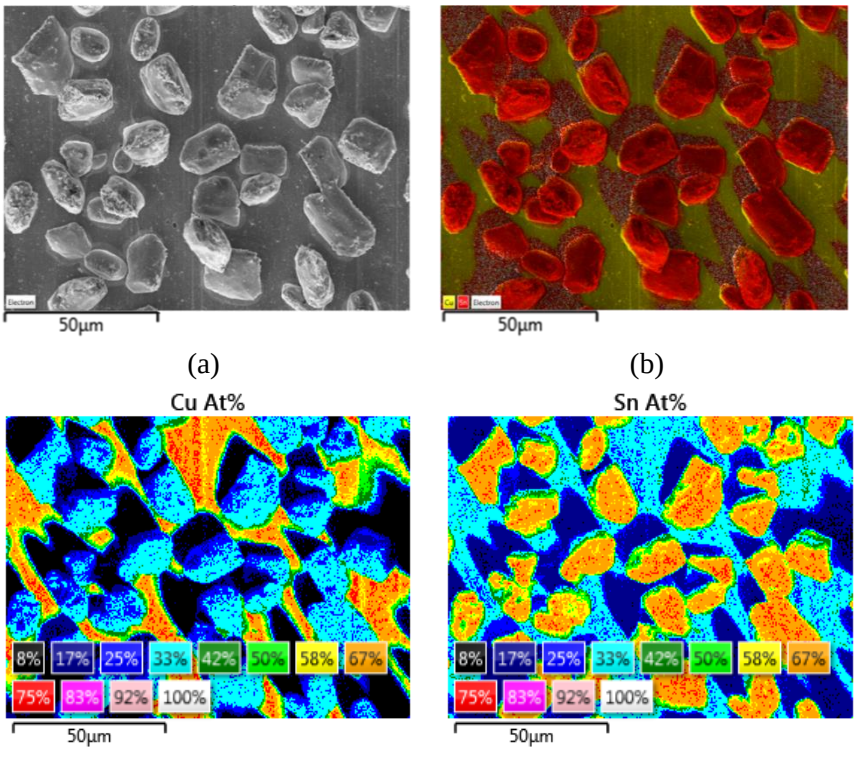

Figure 8.23. SnCuNi-DC alloy on copper substrate after reflowing in the industrial oven (a) SEM micrograph; (b) EDX qualitative map, where tin is represented in red while copper with yellow; (c) and (d) are the EDX quantitative maps representing the distribution of copper and tin in atomic percentage.

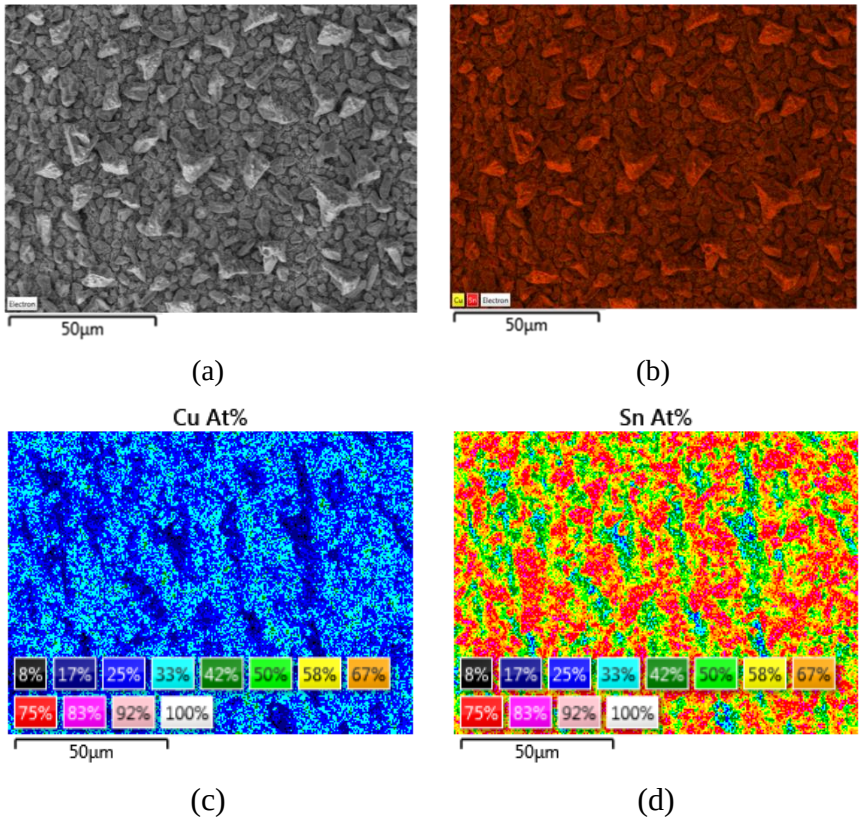

Figure 8.24. SnCuNi-PC alloy on copper substrate after reflowing in the industrial oven (a) SEM micrograph; (b) EDX qualitative map, where tin is represented in red while copper with yellow; (c) and (d) are the EDX quantitative maps representing the distribution of copper and tin in atomic percentage.

On the X-ray analysis, the change is composition observed in the EDX analysis is evidenced by the formation of more Cu_6Sn_5 intermetallic (Card No.: 01-076-2703). Apart from this, the patters look similar to what we have previously obtained before reflowing. Tin, as tetragonal phase (Card No.00-004-0673) $CuNi_2Sn$ (Card No.: 30592) as well as copper (Card No. 00-004-0836) mainly from the substrate were identified.

The anticorrosive properties of the samples prepared under DC and PC mode after reflowing onto the industrial oven were investigated by linear sweep voltammetry (LSV) and electrochemical impedance spectroscopy (EIS) in 0.5 M NaCl at room temperature. Prior to reflowing, SnCuNi-PC exhibited better anticorrosive properties compared to SnCuNi-DC system. However, after reflowing, the anticorrosive properties of the systems changed and the SnCuNi-DC system exhibit better corrosion resistance.

Furthermore, the SnCuNi-DC and SnCuNi-PC systems after reflowing were immersed in 0.1 M NaCl during one-week.

Figures 8.27 and 8.28 illustrate the SEM micrographs of both alloys after 24 h immersion. Corrosion products were observed on the surface of SnCuNi-DC alloy after heating even 24 h posterior to immersion. It is worth to mention that prior reflowing, after 24 h of exposure to aggressive environment no sign of corrosion products was detect. On contrary, the PC sample after reflowing, shows no sign of corrosion, while prior reflowing a formation of a passive film was observed. This phenomenon, again confirms that the reflowing process induces a change in the alloy composition that affects the corrosion resistance as confirmed in the LSV and EIS experiments. If we keep the samples in 0.1 M NaCl solution one-week, the formation of a passive film is observed on both systems (see Figures 8.27 and 8.28).

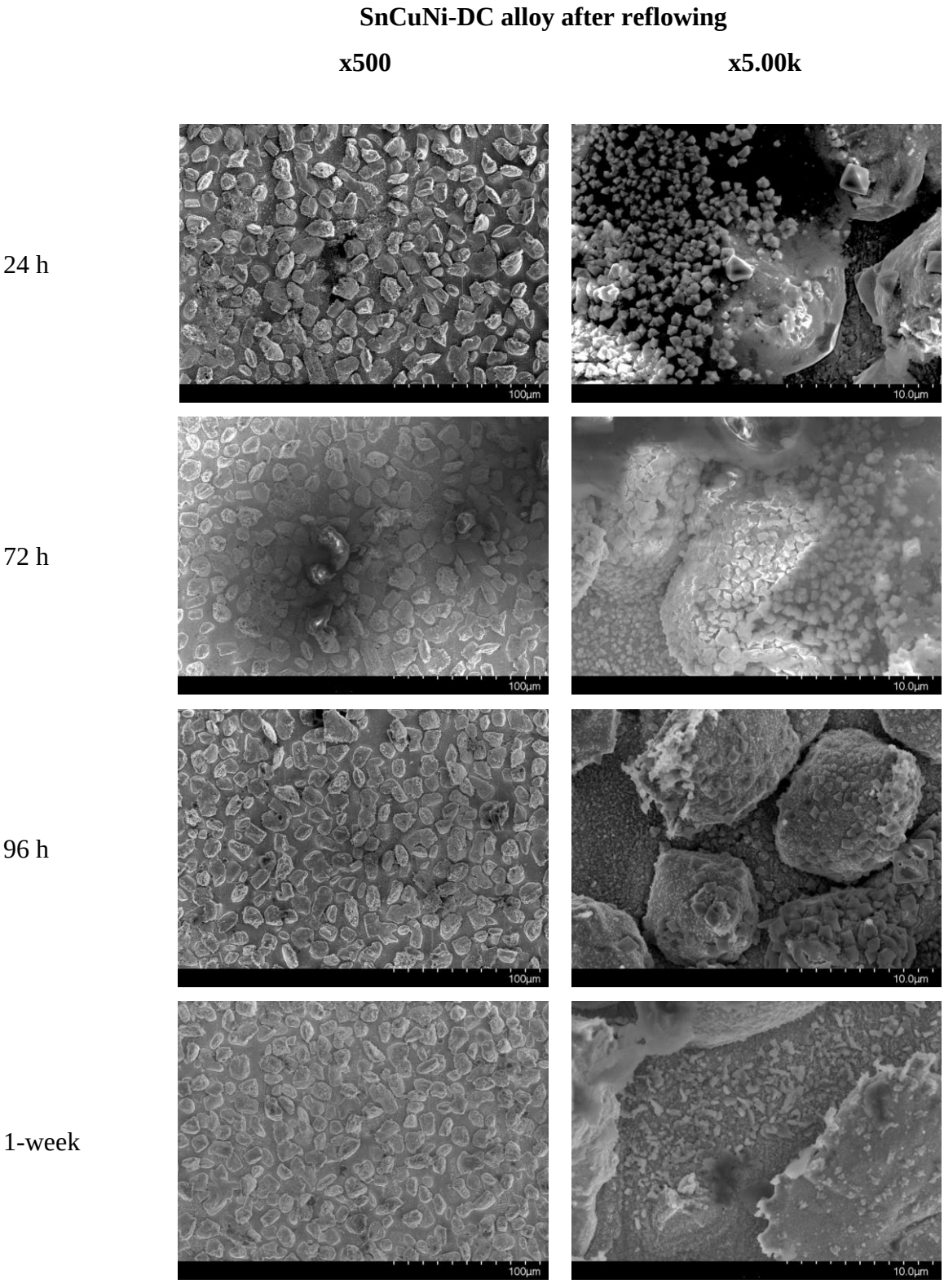

Figure 8.27. SnCuNi-DC alloys after reflowing at different times of immersion in 0.1 M NaCl electrolyte at different magnifications.

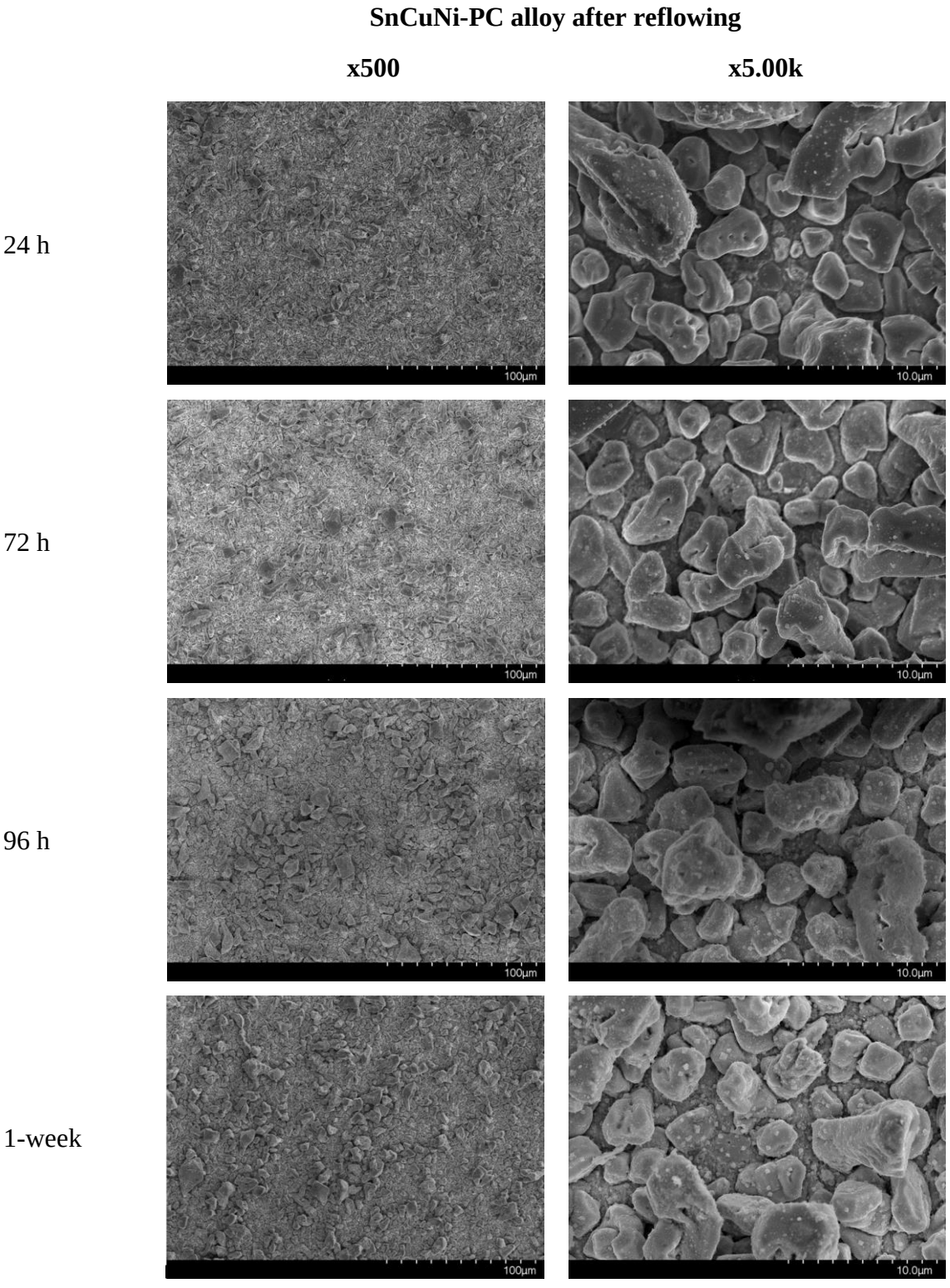

Figure 8.28. SnCuNi-PC alloys after reflowing at different times of immersion in 0.1 M NaCl electrolyte at different magnifications.

Chapter IX: Conclusions

General conclusions

The aim of the thesis was to investigate the electrodeposition of Ni-Sn and Sn-Cu-Ni alloys and Ni-Sn-reduced graphene oxide composite using air and water stable deep eutectic solvents (DESs) as electrolytes. The selected DESs were binary mixtures of choline chloride (ChCl) with either ethylene glycol (named ILEG) or with malonic acid (named ILM). The nucleation mechanisms and influences of operating parameters, especially the direct current (DC) and pulsed current (PC), to the properties of these coatings were studied. Special attention was given to the corrosion protection properties of the films which are investigated at macro-and micro-scale. Since the Sn-Cu-Ni alloy has found applications as lead-free solder in electronic industry, its plating on printed circuit boards and behavior under industrial reflowing conditions were also studied.

The following general conclusions can be drawn from our research:

1. Ni-Sn alloys have been electrodeposited at 75±5 °C on copper substrate from ILEG deep eutectic solvent under both direct current and pulsed current plating modes. *We mention that successful preparation under PC mode is reported for the first time in the literature.* Cyclic voltammetry using glassy carbon electrode clearly evidenced cathodic peaks which may be assigned to the separate deposition of pure metals (Ni, Sn) or to the co-deposition of the NiSn alloy. The current-time transients fitted the theoretical curve associated with instantaneous nucleation and tridimensional growth is controlled by diffusion. We demonstrated by SEM/EDX that no significant changes were observed in the morphology and composition of the deposits independently on the electrolyte composition and the plating mode. Smaller crystallite size and improved mechanical properties were obtained when the Ni-Sn alloy was plated under PC mode. The presence of the metastable phase NiSn (1:1 atomic) was revealed by XRD analysis, whereas an irreversible transformation of NiSn (1:1) into stable Ni_3Sn_2 and Ni_3Sn_4 phases was evidenced by differential scanning calorimetry.

2. Reduced graphene oxide has been successfully incorporated into the metallic matrix of Ni-Sn alloy under pulsed current mode from ILEG deep eutectic solvent. *To the best of our knowledge, this research is the first investigation reporting the electrodeposition and characterization of NiSn-rGO composite coatings involving DESs.* Cyclic voltammograms showed that the presence of GO in the electrolyte does not induce a significant shift of the cathodic peak assigned to the Ni-Sn alloy electrodeposition but its current is slightly higher. The potentiostatic current transients indicate a typical behavior of composite deposition involving an instantaneous nucleation and growth process.Regarding pulse current deposition on Cu, the properties of composite were evidenced by Raman spectroscopy, SEM, including a cross-section SEM, XRD and AFM. It was observed that the increase in the T_{OFF} time led to a better incorporation of the carbon-based material, since the chance of the graphene sheets reaching the cathode is increased. NiSn-rGO composite coatings possess an adequate adhesion to the metallic substrate, have changed surface morphology, a decrease in the crystallite size and an increased surface roughness parameter. The carbon determined by the EDX analysis is originated not only from the rGO sheets but also from the deep eutectic solvent.An improvement in the corrosion properties of the composite film compared with Ni-Sn alloy was assessed by recording of the potentiodynamic polarization curves and the electrochemical impedance spectroscopy (EIS) spectra in aerated 0.5 M NaCl solution. In the first hours of immersion E_{corr} shifted to more positive values, I_{corr} decreased by more than an

order of magnitude and a larger diameter of Nyquist semicircle was observed. However, after longer immersion periods, of 168 and 336 h of exposure, the performances of composite were similar to Ni-Sn alloy coating; this phenomenon might be due to the activation of some defects present on the NiSn-rGO surface (not initially visible). The non-uniform distribution of the rGO within the alloy matrix is not excluded, thus allowing the diffusion of the aggressive Cl^- ions within the layer.

3. Deposition of Sn-Cu-Ni ternary alloy from two types of deep eutectic solvents consisting of either ILM or ILEG was investigated. *It is worth mentioning that the first electrolyte system (choline chloride : malonic acid (1:1 molar ratio) was not investigated until now and has not been reported in literature.* The obtained voltammograms at 60 ^oC in the case of ILM-$SnCl_2$-$CuCl_2$-$NiCl_2$ and ILEG-$SnCl_2$-$CuCl_2$-$NiCl_2$ systems on GC electrode showed a single cathodic peak, that is ascribed to the direct co-deposition of ternary Sn-Cu-Ni alloy. The use of ILEG based electrolytes appeared to facilitate a clearer electrochemical response as compared to ILM one, with well-defined cathodic and anodic peaks. Voltammograms recorded in ILEG containing 50 mM $SnCl_2$ + 0.345 mM $CuCl_2$ + 0.055 mM $NiCl_2$ at various operating temperatures in the range 25–80 ^oC and scan rates between 5 and 100 mV s^{-1} showed that the cathodic process is activated by temperature and occurs through a nucleation mechanism under diffusion-controlled growth. The rising part of the chronoamperograms ($t/t_{max} < 1$) fitted the theoretical curve associated with instantaneous nucleation with three-dimensional growth of the nuclei whatever the applied overpotential. Electrodeposition of Sn-Cu-Ni alloy onto Cu substrate has been performed involving electrolytes with the same concentrations of the metallic salts (500 mM $SnCl_2 \cdot 2H_2O$ + 1.13 mM $NiCl_2 \cdot 6H_2O$ + 3.02 mM $CuCl_2 \cdot 2H_2O$) dissolved either in ILM or ILEG solvent. The same four values of the current density (5-13 mA/cm^2) were applied. Powdery and not adherent Sn-Cu-Ni deposit to the copper substrate was observed using ILM. For ILEG solvent, the composition of the bath was optimized in order to obtain an alloy with a composition similar to the one used industrially (99.25 wt.%Sn+0.7 wt.% Cu+0.05 wt.% Ni). Uniform, adherent, and bright Sn-Cu-Ni alloy coatings have been obtained. The films were plated here only under direct current and SEM micrographs showed an increase of the grain size as compared to the deposits involving ILM. EDX results noticed the decrease of Ni content against the increase of the applied current density, whereas Cu content increased; this might be related to the diffusion coefficients of the two metallic species. The XRD analysis revealed the presence of monoclinic Cu_6Sn_5 and cubic $CuNi_2Sn$ and $(Cu,Ni)_6Sn_5$ intermetallic compounds. Through a fine tuning of the metallic salts concentrations in the electrolytes and of the driven current density it was possible to control the alloy composition, in order to achieve a stoichiometry of Sn99.29-Cu0.65-Ni0.06, very close to that industrially recommended to be used as lead-free solder alloy in electronic industry. According to the TGA measurements the melting point of the electrodeposited Sn99.29-Cu0.65-Ni0.06 alloy was 229 ^oC. Furthermore, the corrosion protection properties of the films were investigated at macro-scale for coatings prepared by DC mode in ILEG. Potentiodynamic polarization plots and EIS spectra corresponding to as-deposited Sn-Cu-Ni alloy (99.29 wt.% Sn, 0.65 wt.% Cu and 0.06 wt.% Ni) coating showed a good corrosion performance, materialized in corrosion current densities of 6-7 µA cm^{-2} and film resistances of about 7625 Ωcm^2, slightly better as compared to the metallurgically prepared lead-free solders having a relatively similar composition.

4. Detailed studies were devoted to the synthesis and characterization Sn-Cu-Ni alloy from ILEG eutectic mixture in pulse plating regime at a fixed average current density and duty cycle, while the pulse frequency was varied. The results were compared with those for Sn-Cu-Ni alloy samples plated under DC from the same electrolyte. *To our best knowledge*,

we have not found any report in the literature on the pulse plating of Sn-Cu-Ni alloys from deep eutectic solvents. SEM micrographs showed that the deposit compactness was improved with decreasing the applied frequency and a diminution in the grain size was detected when pulsed current plating was used. The elemental composition of the Sn-Cu-Ni alloy was also modified when pulse current is applied; for instance, an increase in the Cu and Ni content in Sn-Cu-Ni alloy was observed in PC, thus affecting the melting point of the alloy. Low melting temperatures were found in PC compared to DC by DSC thermal analysis. Comparative anti-corrosive properties of the Sn-Cu-Ni films obtained by DC and PC were investigated at either macro-scale (by potentiodynamic polarization and electrochemical impedance spectroscopy) or micro-scale (by scanning vibrating electrode technique). The analysis revealed that the use of pulsed current improved the corrosion performance of the alloy. Although E_{corr} for both samples was quite similar, the corrosion current was lower for the sample prepared by PC. The larger diameter of Nyquist curve for sample prepared in pulse means a lower corrosion current than for sample prepared in DC. SVET technique showed that there was observed a galvanic coupling between the alloy coating, which mainly contains Sn, and the metallic Cu from the substrate. Also, it was observed by SVET technique that, immediately after immersion in 0.1 M NaCl solution, the value of the integrated anodic current is similar in magnitude in both samples prepared by DC and PC, but after 24 h of immersion the anodic currents are higher in the case of DC sample compared to the sample from PC deposition, which clearly indicates a poor corrosion behavior of this sample. However, after 1-week immersion it was seen for both samples prepared by DC and PC a decrease in the anodic current density determined by SVET, indicating the possible formation of a passive film. The corrosion products formed after 1-week immersion were investigated by Raman spectroscopy. The cathode-to-anode surface ratio expressed by $A_{exposed\ substrate}/A_{coated\ substrate}$ ratio was found higher in DC than in the PC sample, thus influencing the galvanic coupling between Sn, from the alloy, and Cu, from the substrate. Lower galvanic coupling was found on PC system compared to DC. After one-week immersion in aggressive NaCl electrolyte on the surface of the PC sample a continuous passive film was observed, while for DC crystals containing tin and oxygen were found randomly distributed on the surface. The corrosion products analyzed by Raman spectroscopy indicated the presence of $Sn_3O_2(OH)_{2-x}Cl_x$, SnO_x as well as SnO_2 species.

5. To illustrate the suitability for its use as solderable coatings in electronic industry, the electrodeposition of Sn-Cu-Ni ternary alloy from ILEG deep eutectic solvent has been successfully scaled-up on printed circuit boards (PCBs) on the pilot plant under DC and PC optimized conditions. The Sn-Cu-Ni coatings were exposed to reflowing conditions into the industrial oven at MIBATRON S.R.L company. After reflowing, the composition of the coating changed, more copper was observed in the grains and more Cu_6Sn_5 intermetallic is detected. The corrosion protection properties were investigated by salt spray test according to the international standards. The PCBs coated with the ternary alloy under pulsed current mode exhibited better corrosion performance. However, the corrosion performance after reflowing was better for the sample prepared under direct current conditions. Further experiments at micro-scale should be performed to a better understanding of the corrosion mechanisms.

6. It is important to point out the novelties presented in this thesis since, based on our literature investigations, the synthesis of Ni-Sn alloys by pulsed current, the preparation of the Ni-Sn-rGO composite material and the electrodeposition of the ternary Sn-Cu-Ni alloy, all electrodeposited from deep eutectic solvents are reported for the first time here.

Future perspectives

The results presented in this thesis showed that Ni-Sn, Ni-Sn-rGO composite and ternary Sn-Cu-Ni alloys can be successfully obtained by electrodeposition from deep eutectic solvents plating baths. A comprehensive investigation of the properties of the films have been detailed.

Significant attention to the anti-corrosive properties of the films has been presented, involving macro- and micro- scale characterization. The micro-scale investigations were related to the ternary Sn-Cu-Ni alloy. It is important to continue the localized corrosion investigations for the binary DESs systems, especially regarding the composite material Ni-Sn-rGO, in order to reveal the role of reduced graphene oxide sheets, responsible for the observed improvement in the anti-corrosive properties of the nickel-tin alloy. The recent acquisition of an electrochemical cell for the atomic force microscopy system (EC-AFM) will allow us to conduct these investigations. Also, the localized corrosion studies of the ternary system will be completed using this analysis.

On the other hand, scant information can be found in literature related to the electrodeposition of ternary alloys from deep eutectic solvents. There is still room to explore new types of alloys from DESs. The use of pulsed current has been shown to improve the hardness and the corrosion performance of the deposits. For this reason, the electrodeposition of ternary alloys films will be studied comparatively using similar procedures. The addition of iron to Ni-Sn alloy could be a good candidate to improve the anti-corrosive properties of the films. The ternary alloy (Ni-Sn-Fe) has been reported for the first time in literature in 2010.

Finally, the expertise acquired on the scale-up electrodeposition of Sn-Cu-Ni alloy from deep eutectic solvent can be expanded to other binary and ternary alloys.

References (selection)

Introduction

[1] G. Z. Yuliy D. Gamburg, *Theory and Practice of Metal Electrodeposition*. 2011.

[2] B. Cornelius, S. Treivish, Y. Rosenthal, and M. Pecht, "Microelectronics Reliability The phenomenon of tin pest : A review," vol. 79, pp. 175–192, 2017, doi: 10.1016/j.microrel.2017.10.030.

[3] J. W. Osenbach, "Tin Whiskers : An Illustrated Guide to Growth Mechanisms and Morphologies," pp. 57–60, 2011, doi: 10.1007/S11837-011-0177-0.

[4] C. M. Whittington and W. Y. Lo, "'Nickel Allergy' arising from decorative nickel plated and alloyed articles: prevention at source," *Trans. Inst. Met. Finish.*, vol. 97, no. 2, pp. 64–66, 2019, doi: 10.1080/00202967.2019.1570737.

[5] P. Møller, J. B. Rasmussen, and S. Kohler, "Electroplated Tin-Nickel Coatings as a Replacement for Nickel to Eliminate Nickel Dermatitis.," *Prod. Finish.*, vol. 78, no. 3, pp. 15–24, 2013.

[8] C. T. J. Low and F. C. Walsh, "Electrodeposition of tin, copper and tin-copper alloys from a methanesulfonic acid electrolyte containing a perfluorinated cationic surfactant," *Surf. Coatings Technol.*, vol. 202, no. 8, pp. 1339–1349, 2008, doi: 10.1016/j.surfcoat.2007.06.032.

[9] Y. Deo, S. Guha, K. Sarkar, P. Mohanta, and D. Pradhan, "Applied Surface Science Electrodeposited Ni-Cu alloy coatings on mild steel for enhanced corrosion properties," *Appl. Surf. Sci.*, vol. 515, pp. 146078, 2020, doi: 10.1016/j.apsusc.2020.146078.

[10] V. Andruch, "Deep eutectic solvents vs ionic liquids : Similarities and differences," vol. 159, 2020, doi: 10.1016/j.microc.2020.105539.

[11] F. I. Danilov and V. S. Protsenko, "Electrodeposition of composite coatings using electrolytes based on deep eutectic solvents: A mini-review," *Vopr. Khimii i Khimicheskoi Tekhnologii*, no. 1, pp. 13–21, 2018.

Chapter IV

[31] H. Rooksby "An X-ray study of tin-nickel electrodeposits". *Trans. IMF* 1950, *27:1*, 153–169.

[35] P. Dutta, M. Clarke, "Structure and thermal stability of tin-nickel alloys electrodeposited from acid baths". *Trans. IMF* 1968, *46*, 20–25.

[42] S. Mohan and N. Rajasekaran "Pulse electrodeposition of tin from sulphate bath". *Surf. Eng.* 2009, 25, 634–638

[43] **S. Rosoiu,** A. Pantazi, A. Petica, A. Cojocaru, S. Costovici, C. Zanella, T. Visan, L. Anicai, and M. Enachescu "Comparative Study of Ni-Sn Alloys Electrodeposited from Choline Chloride-Based Ionic Liquids in Direct and Pulsed Current", *Coatings*, vol. 9, no. 12, p. 801, 2019. doi: 10.3390/coatings9120801

[44] P. Møller, J. Boyce, L. P. Nielsen "Electroplated Tin-Nickel Coatings as a Replacement for Nickel to Eliminate Nickel Dermatitis", NASF Surface Technology White Papers, 78, 3, 15-24, 2013

Chapter V

[31] A.T.S.C. Brandão, L. Anicai, O. A. Lazar, **S. Rosoiu**, A. Pantazi, R. Costa, M. Enachescu, C.M. Pereira and A.F. Silva, "Electrodeposition of Sn and Sn composites with carbon materials using choline chloride-based ionic liquids". *Coatings* 2019, *9*, 798.

[47] A. Eckmann, A. Felten, A. Mishchenko, L. Britnell, R. Krupke, K. Novoselov and C.Casiraghi, "Probing the nature of defects in graphene by Raman spectroscopy". *Nano Lett.* 2012, *12*, 3925–3930.

[48] A. Marrani, R. Zanoni, R. Schrebler and E. Dalchiele, "Toward graphene/silicon interface via controlled electrochemical reduction of graphene oxide". *J. Phys. Chem. C* 2017, *121*, 5675–5683.

[50] H. Rooksby, "An X-Ray study of tin-nickel electrodeposits". *Trans. IMF* 1950, *27*, 153–169

[51] J. Chen, J. Li, D. Xiong, Y. He, Y. Ji and Y. Qin, "Preparation and tribological behavior of Ni-graphene composite coating under room temperature". *Appl. Surf. Sci.* 2016, *361*, 49–56.

[54] D. Zheng, M. Li, Y. Li, C. Qin, Y. Wang and Z.A. Wang, "$Ni(OH)_2$ nanopetals network for high-performance supercapacitors synthesized by immersing Ni nanofoam in water". *Beilstein J. Nanotechnol.* 2019, *10*, 281–293

[55] A. Marinoiu, G. Mihai, O. Lazar, **S. Rosoiu**, M. Prodana, C. Sisu, M. Raceanu, M. Enachescu "Facile preparation of graphene-supported platinum-cobalt nanoparticles and their use as electrocatalyst in pem fuel cells". Nanomaterials –functional properties and applications. Editura Academiei Romane; Bucharest 2020, 9-38

[56] A.T. Brandão, **S. Rosoiu**, R. Costa, O. Lazar, A. Silva, L. Anicai, C. Pereira and M. Enachescu, "Characterization and electrochemical studies of MWCNTs decorated with Ag nanoparticles through pulse reversed current electrodeposition using a deep eutectic solvent for energy storage applications",*Journal of Materials Research and Technology*, 2021. doi: 10.1016/j.jmrt.2021.08.031

[57] **S. Rosoiu**, A. Pantazi, A. Petica, A. Cojocaru, S. Costovici, C. Zanella, T. Visan, L. Anicai, and M. Enachescu, "Electrodeposition of NiSn-rGO Composite Coatings from Deep Eutectic Solvents and Their Physicochemical Characterization", *Metals*, vol. 10, no. 11, p. 1455, 2020. doi: 10.3390/met10111455

Chapter VI

[13] K. Nogita, T. Nishimura, "Nickel-stabilized hexagonal (Cu, Ni)6Sn5 in Sn–Cu–Ni lead-free solder alloys", *Scripta Mater.*, 59(2), 2008, 191-194. Doi: 10.1016/j.scriptamat.2008.03.002

[14] T. Ventura, Y. Cho, A.K. Dahle, "Solidification mechanisms in the Sn-Cu-Ni lead-free solder system", *Mater. Sci. Forum*, Vols. 654-656, *J.F. Nie, A. Morton, Eds*., 2010, 1381-1384. Doi: 10.4028/www.scientific.net/MSF.654-656.1381

[46] L. Anicai,,A. Petica, S. Costovici, P. Prioteasa, T. Visan, "Electrodeposition of Sn and NiSn alloys coatings using choline chloride based ionic liquids—Evaluation of corrosion behavior", *Electrochim. Acta*, 114, 2013, 868-877. Doi: 10.1016/j.electacta.2013.08.043

[67] S. Rao, X. Zou, S. Wang, T. Shi, Y. Lu, L. Ji, H.Y. Hsu, Q. Xu, X. Lu, "Electrodeposition of porous Sn-Ni-Cu alloy anode for lithium-ion batteries from nickel matte in deep eutectic solvents", *J. Electrochem. Soc.*, 166(1), 2019, D427. Doi: 10.1149/2.0881910jes

[72] **S. Rosoiu**, A.G. Pantazi, A. Petica, A. Cojocaru, S. Costovici, C. Zanella, T. Visan, L.Anicai, M. Enachescu, "Electrodeposition of NiSn-rGO composite coatings from deep eutectic solvents and their physicochemical characterization", *Metals*, 10(11), 2020, 1455. Doi: 10.3390/met10111455

[78] T. Ventura, C.M. Gourlay, K. Nogita, T. Nishimura, M. Rappaz, A.K. Dahle, "The influence of 0–0.1 wt.% Ni on the microstructure and fluidity length of Sn-0.7Cu-xNi", *J. Electron. Mater.*, 37 2008, 32–39. Doi: 10.1007/s11664-007-0281-7

[79] Balver Zinn solder SN100C, SnCu0.7Ni SN100Ce SnNi, Technical Data Sheet. https://www.balverzinn.com/solder-SN100C.html

[80] A.A. El-Daly, A.E. Hammad, "Enhancement of creep resistance and thermal behavior of eutectic Sn–Cu lead-free solder alloy by Ag and In-additions", *Mater. Des.*, 40, 2012, 292-298; doi: 10.1016/j.matdes.2012.04.007

[81] A.A. El-Daly, A.E. Hammad, "Enhancement of creep resistance and thermal behavior of eutectic Sn–Cu lead-free solder alloy by Ag and In-additions", *Mater. Des.*, 40, 2012, 292-298; doi: 10.1016/j.matdes.2012.04.007,

[82] M. Zhao, L. Zhang, Z.Q. Liu, M.Y. Xiong, L. Sun, "Structure and properties of Sn-Cu lead-free solders in electronics packaging", *Sci. Technol. Adv. Mater.*, 20(1), 2019, 421-444. Doi: 10.1080/14686996.2019.1591168

[83] S. Jayesh, J. Elias, "Experimental investigations on the effect of addition of Ag into ternary lead free solder alloy Sn-1Cu-1Ni", *Lett. Mater.*, 9(2), 2019, 239-242. Doi: 10.22226/2410-3535-2019-2-239-242

[84] J.-E.C. Guerrero, D.H. Camacho, O. Mokhtari, H. Nishikawa, "Corrosion and leaching behaviours of Sn-0.7Cu-0.05Ni lead-free solder in 3.5 wt.% NaCl solution," *Int. J. Corros.*, 2018 Article ID 6580750. doi.org/10.1155/2018/6580750

[85] W. Osório, J. Spinelli, C. Afonso, L. Peixoto, A. Garcia, "Microstructure, corrosion behaviour and microhardness of a directionally solidified Sn–Cu solder alloy." *Electrochim. Acta*, 56(24), 2011 8891-8899. doi.org/10.1016/j.electacta.2011.07.114

[86] W.R. Osorio, L.C. Peixoto, L.R. Garcia, A. Garcia, J.E. Spinelli, "The Effects of Microstructure and Ag3Sn and Cu6Sn5 Intermetallics on the Electrochemical Behavior of Sn-Ag and Sn-Cu Solder" Alloys, *Int. J. Electrochem. Sci.*, 7 2012, 6436 – 6452

[87] S. Sainis, **S. Rosoiu**, E. Ghassemali and C. Zanella, "The role of microstructure and cathodic intermetallics in localised deposition mechanism of conversion compounds on Al (Si, Fe, Cu) alloy", *Surface and Coatings Technology*, vol. 402, p. 126502, 2020. doi: 10.1016/j.surfcoat.2020.126502

Chapter VII

[26] X. Lao, C. Cheng, X. Min, J. Zhao, D. Zhou, L. Wang, and X. Li , "Corrosion and leaching behaviors of Sn-based alloy in simulated soil solutions," *Trans. Nonferrous Met. Soc. China (English Ed.*, vol. 26, no. 2, pp. 581–588, 2016, doi: 10.1016/S1003-6326(16)64146-8.

[28] R. M. Souto, Y. González-García, A. C. Bastos, and A. M. Simões, "Investigating corrosion processes in the micrometric range: A SVET study of the galvanic corrosion of zinc coupled with iron," *Corros. Sci.*, vol. 49, no. 12, pp. 4568–4580, 2007, doi: 10.1016/j.corsci.2007.04.016.

[30] J. Gole, A. Iretskii, M. White, A. Jacob, W. Carter, S. Prokes an A. Erickson, "Suggested oxidation state dependence for the activity of submicron structures prepared from tin/tin oxide mixtures," *Chem. Mater.*, vol. 16, no. 25, pp. 5473–5481, 2004, doi: 10.1021/cm030618i.

[31] P. Eckold, M. Rolff, R. Niewa, and W. Hügel, "Synthesis, characterization and in situ Raman detection of Sn3O2(OH)2-xClx phases as intermediates in tin corrosion," *Corros. Sci.*, vol. 98, pp. 399–405, 2015, doi: 10.1016/j.corsci.2015.05.052.

[32] D. Li, P. P. Conway, and C. Liu, "Corrosion characterization of tin-lead and lead free solders in 3.5 wt.% NaCl solution," *Corros. Sci.*, vol. 50, no. 4, pp. 995–1004, 2008, doi: 10.1016/j.corsci.2007.11.025.

[33] C. Q. Cheng, F. Yang, J. Zhao, L. H. Wang, and X. G. Li, "Leaching of heavy metal elements in solder alloys," *Corros. Sci.*, vol. 53, no. 5, pp. 1738–1747, 2011, doi: 10.1016/j.corsci.2011.01.049

Chapter VIII

[14] B. N. Grgur, *chapter 4: The current distribution in electrochemical cells*, in: Fundamental Aspects of Electrometallurgy, K. Popov, *B. Grgur*, S.S. Djokić, *(*Eds.), Springer, pp. 101–143, 2002, doi: 10.1007/0-306-47564-2_4

Scientific activities

Published articles

1. **S. Rosoiu**, S. Costovici, C. Moise, A.Petica, L. Anicai, T.Visan and M. Enachescu, "Electrodeposition of ternary Sn-Cu-Ni alloys as lead-free solders using deep eutectic solvents" under revision at *Electrochemica Acta*
2. **S. Rosoiu**, A. Pantazi, A. Petica, A. Cojocaru, S. Costovici, C. Zanella, T. Visan, L. Anicai, and M. Enachescu, "Electrodeposition of NiSn-rGO Composite Coatings from Deep Eutectic Solvents and Their Physicochemical Characterization", *Metals*, vol. 10, no. 11, p. 1455, 2020. doi: 10.3390/met10111455 (access)
3. **S. Rosoiu,** A. Pantazi, A. Petica, A. Cojocaru, S. Costovici, C. Zanella, T. Visan, L. Anicai, and M. Enachescu "Comparative Study of Ni-Sn Alloys Electrodeposited from Choline Chloride-Based Ionic Liquids in Direct and Pulsed Current",*Coatings*, vol. 9, no. 12, p. 801, 2019. doi: 10.3390/coatings9120801 (access)
4. A. Brandão, **S. Rosoiu**, R. Costa, O. Lazar, A. Silva, L. Anicai, C. Pereira and M. Enachescu, "Characterization and electrochemical studies of MWCNTs decorated with Ag nanoparticles through pulse reversed current electrodeposition using a deep eutectic solvent for energy storage applications",*Journal of Materials Research and Technology*, 2021. doi: 10.1016/j.jmrt.2021.08.031 (access)
5. C. Moise, L. Enache, V. Anastasoaie, O. Lazar, G. Mihai, S. **Rosoiu,**.M. Bercu, M. Enachescu, "On the growth of copper oxide nanowires by thermal oxidation near the threshold temperature at atmospheric pressure",*Journal of Alloys and Compounds*, vol. 886, p. 161130, 2021. Available: 10.1016/j.jallcom.2021.161130 (access)
6. S. Sainis, **S. Rosoiu**, E. Ghassemali and C. Zanella, "The role of microstructure and cathodic intermetallics in localised deposition mechanism of conversion compounds on Al (Si, Fe, Cu) alloy",*Surface and Coatings Technology*, vol. 402, p. 126502, 2020. doi: 10.1016/j.surfcoat.2020.126502 (access)
7. Marinoiu, G. Mihai, O. Lazar, **S. Rosoiu**, M. Prodana, C. Sisu, M. Raceanu, M. Enachescu "Facile preparation of graphene-supported platinum-cobalt nanoparticles and their use as electrocatalyst in pem fuel cells". Nanomaterials –functional properties and applications. Editura Academiei Romane; Bucharest 2020, 9-38 (access)
8. Brandão, L. Anicai, O. Lazar, **S. Rosoiu**, A. Pantazi, R. Costa, M. Enachescu, C. M. Pereira and A. F. Silva, "Electrodeposition of Sn and Sn Composites with Carbon Materials Using Choline Chloride-Based Ionic Liquids",*Coatings*, vol. 9, no. 12, p. 798, 2019. doi: 10.3390/coatings9120798 (access)
9. G. Mihai, **S. Rosoiu**, S. Costovici, L. Anicai, M. Enachescu "Synthesis of copper nanowires using aqueous and ionic liquid electrolytes for electrochemical detection". *U.P.B. Sci. Bull., Series B*, Vol. 81, Iss. 2, 2019 (access)

Articles under preparation:

1. **S. Rosoiu** *et al.* "Corrosion behavior of Sn-Cu-Ni lead-free solders from deep eutectic solvents"
2. **S. Rosoiu** *et al.* "Electrodeposition of Sn-Cu-Ni alloy on printed circuit board from deep eutectic solvent using a pilot-scale setup"

Scientific conferences

1. **S. Rosoiu**, S. Costovici, G. Mihai, M. Mousavib, Y. G. Garcia, L. Anicai, T. Visan, M. Enachescu "Corrosion behavior of the ternary Sn-Cu-Ni lead-free solders from deep eutectic solvents", 72nd Annual Meeting of the International Society of Electrochemistry ISE 2021, Jeju, Korea (Oral Presentation)
2. **S. Rosoiu**, S. Costovici, G. Mihaia, Y. G. Garcia, L. Anicai, T. Visan, M. Enachescu "Evaluation of corrosion behavior of the ternary Sn-Ni-Cu alloy coatings obtained from deep eutectic solvents", Eurocorr 2021, Budapest, Hungary (Poster)
3. **S. Rosoiu**, S. Costovici, C. Moise, L. Anicai, T. Visan, M. Enachescu "Electrodeposition of ternary Sn-Cu-Ni alloys as lead-free solders using Deep Eutectic Solvents", Eurocorr 2020, Brussels, Belgium (Oral Presentation)
4. **S. Rosoiu**, S. Costovici, C. Moise, L. Anicai, T. Visan, M. Enachescu "Sn-Cu-Ni Ternary Alloy Solders Electrodeposited from Deep Eutectic Solvents", 71st Annual Meeting of the International Society of Electrochemistry ISE 2020, Belgrad, Serbia (Poster)
5. **S. Rosoiu**, A. Petica, A. G. Pantazi, M. Enachescu, T. Visan, L. Anicai "Electrodeposition of Ag and Ag composites with carbon nanotubes using novel deep eutectic solvent formulations", Regional Symposium on Electrochemistry of South-East Europe RSE SEE-7 2019, Split, Croatia (**3rd oral presentation award**)
6. **S. Rosoiu**, A. G. Pantazi, A. Petica, A. Cojocaru, C. Zanella, M. Enachescu, S. Costovici, T. Visan, L. Anicai "Electrodeposition of Ni-Sn alloys and Ni-Sn / rGO composite coatings from deep eutectic solvents and their physicochemical characterization" Electrochem 2019, Glasgow, UK (Oral presentation)
7. **S. Rosoiu**, A. G. Pantazi, A. Petica, A. Cojocaru, S. Costovici, T. Visan, L. Anicai, M. Enachescu "Electrodeposition of Ni-Sn Alloy/rGO Composite Coatings Involving Choline Chloride Based Deep Eutectic Solvents" 21st Romanian International Conference on Chemistry and Chemical Engineering RICCE 2019, Mamaia, Romania (Oral presentation)
8. **S. Rosoiu**, A. G. Pantazi, A. Petica, A. Cojocaru, S. Costovici, T. Visan, L. Anicai, M. Enachescu "Ni-Sn alloy/ rGO composite coatings involving deep eutectic solvents – Evaluation of corrosion behavior", Eurocorr 2019, Seville, Spain (Poster presentation)
9. **S. Rosoiu**, A.G. Pantazi, A. Petica, A. Cojocaru, S. Costovici, T. Visan, M. Enachescu, L. Anicai "Morphological and structural investigations of electrodeposited Ni-Sn alloy/reduced graphene oxide composites from deep eutectic solvents", Multi-Functional Nano-Carbon Composite Materials 2018 COST Action, Bucharest, Romania (Poster)
10. G. Mihai, C. Moise, O. Lazar, V. Anastasoaie, L. B. Enache, **S. Rosoiu**, M. Vardaki, A. Pantazi, M. Enachescu "GaN Nanostructuring" NOMARES 2020 (Oral Presentation)
11. L. Anicai, S. Costovici, **S. Rosoiu**, C. Moise, T. Visan " Electrodeposition of Sn Based Ternary Alloys Using Deep Eutectic Solvents" 21st Romanian International Conference on Chemistry and Chemical Engineering RICCE 2019, Mamaia, Romania (Oral presentation)

12. Anca Cojocaru, S. Rosoiu, O. Lazar, G. Mihai, A. G. Pantazi, M. Enachescu, L. Anicai, T. Visan "Electrodeposition of Nickel-Cobalt Alloy / MWCNT Composite Coatings Involving Deep Eutectic Solvents" 21st Romanian International Conference on Chemistry and Chemical Engineering RICCE 2019, Mamaia, Romania (Poster)
13. A. Pantazi, **S. Rosoiu**, A. Petica, O. Tutunaru, T. Visan, M. Enachescu, L. Anicai "Multiwalled carbon nanotubes-silver nanocomposite coatings from ionic liquids analogues – morphological and structural analysis" Multi- Functional Nano-Carbon Composite Materials 2018 COST Action, Bucharest, Romania (Poster)

Training schools

1. **Innovation and Technology Transfer,** Vrije Universiteit Brussel, 25.05-19.06.2020, Online
2. **Corrosion protection at micro-scale - application fields,** Universidad Autonoma de Barcelona, 18-22.11.2019, Barcelona, Spain
3. **Fundamentals of Corrosion Protection and Coatings Production,** Jožef Stefan Institute, 24-29.06.2019, Ljubljana, Slovenia
4. **Nanomaterials synthesis and advanced characterization techniques at nanometer and atomic scale** COST Action 15107, Center for Surface Science and Nanotechnology-University Politehnica of Bucharest, 04-07.06.2019, Bucharest, Romania
5. **Structural, mechanical and surface analytical techniques,** Jönköping University, 06-09.11.2018, Jönköping, Sweden
6. **Fundamentals of electrochemistry and corrosion mechanisms,** Delft University of Technology, 15-20.07.2018, Delft, Netherlands

Research internships

1. Localized corrosion characterization of Ni and Sn based alloys, **Delft University of Technology**, 10.2020 12.2020, Delft, Netherlands
2. Characterization of Ni and Sn based alloys, **Jönköping University**, 04.2019-05.2019 and 08.2020-09.2020, Jönköping, Sweden